nature communications

Article

https://doi.org/10.1038/s41467-024-54244-8

Lateral prefrontal theta oscillations causally drive a computational mechanism underlying conflict expectation and adaptation

Received: 21 May 2024

Accepted: 1 November 2024

Published online: 14 November 2024

Check for updates

María Paz Martínez-Molina[1], Gabriela Valdebenito-Oyarzo[1], Patricia Soto-Icaza[1], Francisco Zamorano[2,3], Alejandra Figueroa-Vargas[1,4], Patricio Carvajal-Paredes[1], Ximena Stecher[5], César Salinas[5], Antoni Valero-Cabré[6,7,8], Rafael Polania[9] & Pablo Billeke[1]

Adapting our behavior to environmental demands relies on our capacity to perceive and manage potential conflicts within our surroundings. While evidence implicates the involvement of the lateral prefrontal cortex and theta oscillations in detecting conflict stimuli, their causal role in conflict expectation remains elusive. Consequently, the exact computations and neural mechanisms underlying these cognitive processes still need to be determined. We employed an integrative approach involving cognitive computational modeling, fMRI, TMS, and EEG to establish a causal link between oscillatory brain function, its neurocomputational role, and the resulting conflict processing and adaptation behavior. Our results reveal a computational process underlying conflict expectation, which correlates with BOLD-fMRI and theta activity in the superior frontal gyrus (SFG). Modulation of theta activity via rhythmic TMS applied over the SFG induces endogenous theta activity, which in turn enhances computations associated with conflict expectation. These findings provide evidence for the causal involvement of SFG theta activity in learning and allocating cognitive resources to address forthcoming conflict stimuli.

In our daily lives, we often encounter environmental challenges that require us to navigate and anticipate conflict situations—for example, determining when to adjust our driving speed to safely maneuver through traffic signals indicating potential hazards, even when running late for work. In such situations, it is necessary to learn about the possibility of difficult situations and allocate cognitive resources to deal with them[1–3]. Crucially, we can integrate previously occurring events to anticipate the need for behavioral control; this process is

[1]Laboratorio de Neurociencia Social y Neuromodulación, Centro de Investigación en Complejidad Social, (neuroCICS), Facultad de Gobierno, Universidad del Desarrollo, Santiago, Chile. [2]Unidad de Neuroimágenes Cuantitativas avanzadas (UNICA), Departamento de Imágenes, Clínica Alemana, Santiago, Chile. [3]Facultad de Ciencias para el Cuidado de la Salud, Campus Los Leones, Universidad San Sebastián, Santiago, Chile. [4]Laboratory for Cognitive and Evolutionary Neuroscience, Centro de Neurociencia Interdisciplinario, Facultad de Medicina, Pontificia Universidad Católica de Chile, Santiago, Chile. [5]Departamento de Imágenes, Facultad de Medicina Clínica Alemana-Universidad del Desarrollo, Santiago, Chile. [6]Causal Dynamics, Plasticity and Rehabilitation Group, FRONTLAB team, Institut du Cerveau et de la Moelle Epinière (ICM), CNRS UMR 7225, INSERM U 1127 and Sorbonne Université, Paris, France. [7]Laboratory for Cerebral Dynamics Plasticity and Rehabilitation, School of Medicine, Boston University, Boston, MA, USA. [8]Cognitive Neuroscience and Information Technology Research Program, Open University of Catalonia (UOC), Barcelona, Spain. [9]Decision Neuroscience Lab, Department of Health Sciences and Technology, ETH Zurich, Zurich, Switzerland. e-mail: pbilleke@udd.cl

commonly called conflict adaptation or proactive cognitive control[4,5]. Conflict adaptation involves integrating past events and experiences to adjust goal-directed actions and improve the control required for upcoming stimuli. Clinical literature has identified that alteration in this processing is a component of multiple pathways that contribute to the development of symptoms in various neuropsychiatric disorders[5,6] such as attention deficit hyperactivity disorder[7], depression[8], bipolar depression[9], obsessive-compulsive disorder[10], Parkinson's disease[11], and schizophrenia[12–14]. However, the conventional evaluation of this process, using, for example, the sequence effects in cognitive tasks, does not show robust evidence for a unitary processing[15–17], presenting disparate results across multiple experimental studies[18–21]. Additionally, simple concepts such as proactive cognitive control may oversimplify a more intricate and integrative processing required to anticipate and navigate environmental stimuli[22–25]. Hence, while conflict adaptation is widely acknowledged as crucial for our adaptation to real-life situations, the evidence remains inconclusive, primarily due to a lack of comprehensive computational understanding of how this processing occurs[26–28]. Hence, unraveling the brain mechanisms underlying this process is critical to objectively developing intervention strategies. Despite ongoing research efforts, the exact computations and neurobiological mechanisms that underlie the expectation of conflict are still not fully understood.

Neuroimaging studies have underscored the significance of the lateral prefrontal cortex in situations where organisms require flexible cognitive control[29]. Lateral prefrontal activity correlates with behavior regulation according to the current perceptual context and the temporal sequences in which stimuli occur[2,30]. Context adaptation and its deficit have been associated with the dorsolateral prefrontal cortex[14,31]. Neurophysiological studies have emphasized the role of oscillatory activity in theta range in several aspects of cognitive control, including its deficit in pathologies[7,32–37]. For instance, oscillatory activity in the theta band over the frontal midline is associated with detecting, communicating, and implementing cognitive control[32,38]. Theta oscillations have been tied to adaptive control mechanisms during response conflict[38]. In addition, conflict anticipation positively correlates with the low-theta band's power[39]. Despite this evidence, the specific computational processes that underlie conflict anticipations and adaptation and whether they are causally implemented by theta activity in prefrontal areas remain unclear.

Here, we tested the hypothesis that theta oscillatory activity in the lateral prefrontal cortex plays a causal role in computing conflict expectation and adaptation. We anticipate that at the behavioral level, reaction time will increase as the expectation of a conflicting event rises in accordance with specific learning computations. The conflict expectation should be reflected in an adaptation of cognitive control during conflict stimuli. At the neural level, we anticipate that the lateral prefrontal brain network correlates with the conflict expectation computations. Additionally, we hypothesized that non-invasive brain stimulation at theta frequency over the lateral prefrontal cortex enhances the effect of conflict expectation. We conducted three sequential experiments using tasks that induce conflict expectations to test these hypotheses. First, we modeled reaction times to identify a candidate computation process underlying conflict expectations. Second, we used functional magnetic resonance imaging (fMRI) to identify brain areas correlating with this candidate computation. Finally, in a concomitant transcranial magnetic stimulation (TMS) and electroencephalography (EEG) experiment, we tested the causal role of theta activity in the identified brain areas in solving conflict expectations (see Supplementary Fig. 1).

Results

Modeling conflict expectation

An illustrative example of situations that generate conflict expectation is provided by the Go-Nogo (GNG) task (Fig. 1B). This task requires inhibitory responses to rapid and infrequent Nogo stimuli. In such a context, as more consecutive Go stimuli occur, there is a higher probability that a Nogo stimulus will occur in the next trial. The expectation of the occurrence of conflict stimuli involves controlling the response, generating longer reaction times for Go stimuli. Such expectations can be based on specific context features, such as the number of preceding Go stimuli[7,40]. Thus, the context of recent stimuli can be integrated to improve the inhibitory response to Nogo stimuli[39]. Thus, expectation can influence processing before the occurrence of conflict stimuli, which differs from the more commonly studied Gratton effect, where adaptive slowing in reaction time occurs after the conflict has taken place[41,42]. We anticipate that subjects will adapt their cognitive control based on the estimated probability of encountering conflicting stimuli (Nogo stimuli) and their expectation in the context of previous stimuli. To investigate this, and building on prior research[7,40], we tested several behavioral models using a sample of 30 subjects who performed the task.

We used reaction time as a proxy for cognitive control and assessed Drift Diffusion Model[43] (DDM or Wiener process). Cognitive control in inhibitory tasks, such as the Go-Nogo paradigm, has been proposed to primarily affect speed-accuracy trade-off that is expressed in the decision boundary (or threshold) in decision-making processes[44]. In line with this theoretical framework, all tested models were designed to modulate the boundary parameter (see Methods). In a null model (M0), we included all relevant regressors except conflict expectation. These regressors encompassed the anticipated slowing of response following errors, categorized as previous commission errors (pCE) and previous omission errors (pOE).

$$\mathrm{M0}: \mathrm{RT} \sim \beta_0 + \beta_2 \mathrm{pCE} + \beta_3 \mathrm{pOE} \quad (1)$$

Then, in the first cognitive model (M1), we hypothesize that the expectation of conflict stimuli (Ex) linearly increases with the number of consecutive Go stimuli in a sequence (nSeq) of stimuli, such that Ex = nSeq.

$$\mathrm{M1}: \mathrm{RT} \sim \beta_0 + \beta_1 \mathrm{Ex} + \beta_2 \mathrm{pCE} + \beta_3 \mathrm{pOE} \quad (2)$$

In the second model (M2), the expectation of conflict stimuli (Ex) is determined by the rational calculation of the probability of the occurrence of the given sequence of Go stimuli, as expressed in the following equation:

$$\mathrm{M2}: \mathrm{Ex} = 1 - (1 - Q)^{(\mathrm{nSeq}-1)} \quad (3)$$

In the preceding equation, Q represents the rate of occurrence of conflicting stimuli, which, for the M2 model, was set to 0.25 (the programmed rate of Nogo stimuli). The −1 in the exponent indicates the impossibility, known by the subject, of the occurrence of two consecutive Nogo stimuli. In other words, the probability of Nogo stimuli occurring in the first position in the sequence is zero. These equations generate a monotonic, yet nonlinear, increase in expectation throughout the sequences of Go stimuli (see Supplementary Fig. 2).

In the third model (M3(seq)), in addition to Eq. 3, we expected that participants learn the rate of occurrence of conflict stimuli, Q, using a learning algorithm as follows.

$$\mathrm{M3}: Q_t = Q_{t-1} + \alpha(C_{t-1} - Q_{t-1}) \quad (4)$$

In the preceding equation, α represents the learning rate, and C_{t-1} indicates the presence ($C_{t-1} = 1$) or absence ($C_{t-1} = 0$) of a conflicting stimulus in the prior trial. Thus, as Q begins to decrease throughout the sequences of Go stimuli, the expectation increases in the first trials but decreases in the later trials of long sequences (see Fig. 1A and Supplementary Fig. 2). We also tested a variation of Model 3 (M3(Q)),

https://doi.org/10.1038/s41467-024-54244-8

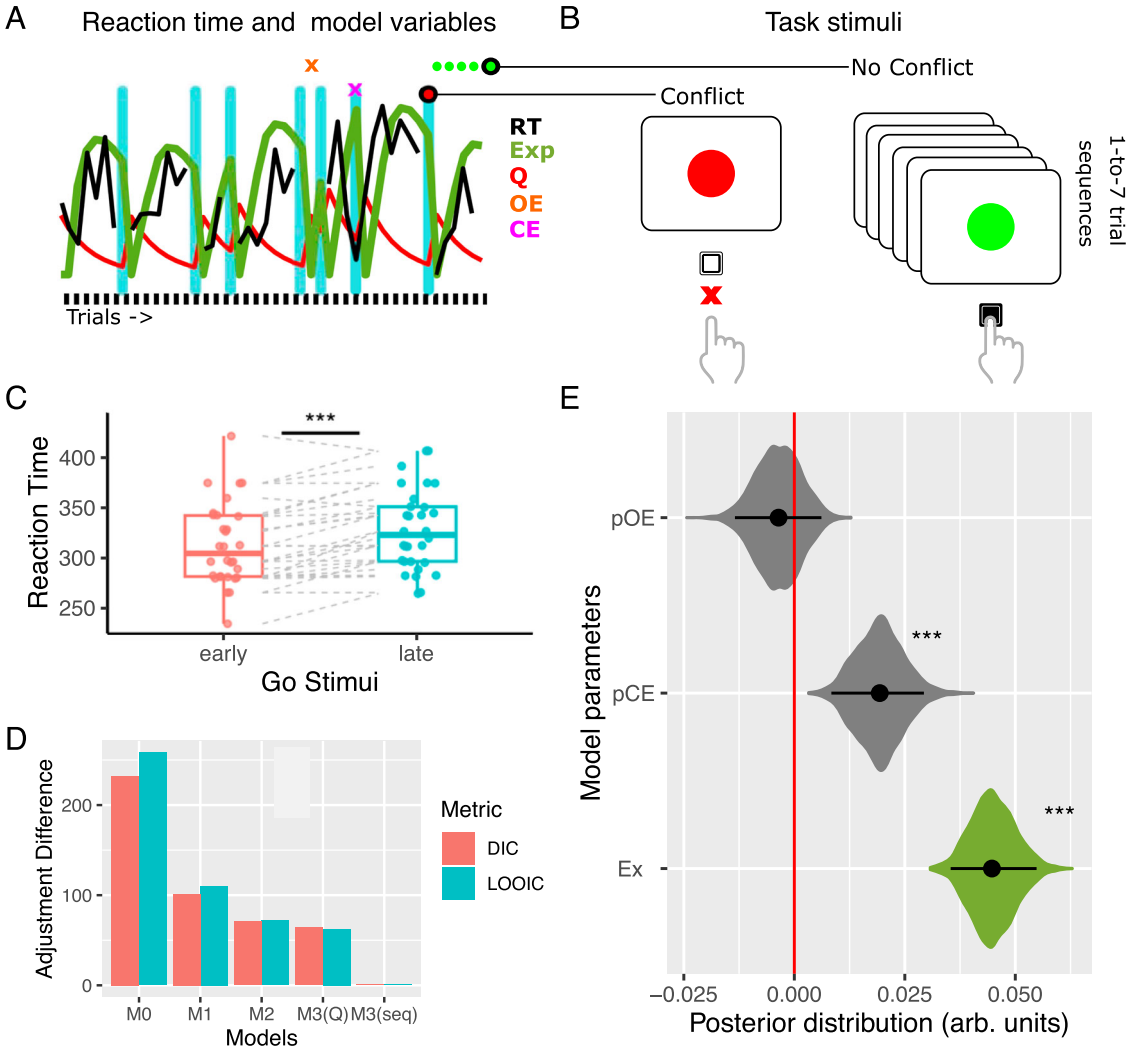

Fig. 1 | Behavioral analysis of Go-Nogo task. A Single-trial example of reaction time and model variables. **B** Go-Nogo Task. **C** Reaction time comparison between the first Go trials (early) and the last Go trial (late) of a sequence ($n = 30$ participants, Wilcoxon test, two-sided, $p = 8.8e\text{-}5$). Boxplots display the extreme values, interquartile range, and median, and each point representing the mean for an individual subject. **D** Models comparison. **E** Posterior distribution of model parameters (Bayesian hypothesis test using p_{MCMC}, two-sided, $p < 0.001$). Black dots represent the mean of the distribution, and black lines represent the 95% high-density intervals. The colored areas represent the complete posterior distribution. * indicates $p < 0.05$, $^{**}p < 0.01$,$^{***}p < 0.001$.CE commission error, DIC deviance information criteria, Ex conflict expectation, OE omission error. pCE previous commission error, pOE previous omission error, RT reaction time. See also Supplementary Tables 1 and 2. Source data are provided as a SourceData file.

which is similar to M3(seq) but with Ex equal to Q instead of using Eq. 3, as proposed in conflict tasks with longer interstimulus intervals[39,45]. Additionally, we tested the lognormal distribution rather than the Wiener process as the link function to explain reaction time variability (see Supplementary Fig. 4).

Behavioral experiment: conflict expectation effect

Initially, we analyzed the impact of expectation modulation on behavior in a sample of 30 healthy participants. We compared the RT for the first two Go stimuli in a sequence with the subsequent three Go stimuli (i.e., 1st and 2nd vs. 3rd, 4th, and 5th stimuli). This division ensured a relatively balanced distribution of trials for comparison (52.3% vs. 47.7%). Our results revealed that the RTs for the initial trials were significantly faster and less accurate than the final trials (RT: mean differences −14.3 ms, confidence interval (CI) = [−19.9 −8.6], Wilcoxon test, $p = 8.8e\text{-}5$, effect size $r = 0.7$; accuracy rates: differences 0.08, CI = [0.06 0.1], Wilcoxon test, $p = 1.8e\text{-}6$, effect size $r = 0.8$). These results suggest that the subjects adjusted their cognitive control, altering the speed-accuracy trade-off.

We then applied the models described in the previous section to evaluate which formulation best explained the mechanism underlying the increase in RT associated with the expectation of conflict stimuli. Among the different models tested, the best-fitted model was M3(seq) (DDM, i.e., Wiener process, see Table 1, Supplementary Tables 1 and 2, and Supplemenatry Fig. 3 for detailed adjustment metrics and graphical representations of the model fit). In this model, the regressor of conflict expectation had a significant impact on reaction time (β_1 Expectation mean = 44.7, 95% high-density interval (HDI) of [35 54], $p_{MCMC} < 0.001$, p_{MCMC} is a p-value derived by comparing the posterior distributions of the estimated parameters sampled via Markov Chain Monte Carlo, see Methods). Additionally, commission error, which refers to the previous error in a Nogo stimulus, was found to significantly increase the reaction time for the Go stimuli (β_2 pCE mean = 19.3, HDI = [8 29.3], $p_{MCMC} < 0.001$). However, no significant effects were found for a pOE (beta pOE mean = −3.6, HDI = [−13 6], $p_{MCMC} = 0.49$, Fig. 1D). The posterior distribution of the learning rate revealed an mean value of 0.29 and an HDI of [0.22 0.37]. Then, we tested if the expectancy of conflict stimuli significantly influenced

Table 1 | Summary of the models and their indicators of adjustment

Model	Linking function	Free parameters	DIC	LOOIC
M0 null	Wiener	5 (3 betas [boundary], drift, tau)	233.0	257.5
M1 linear	Wiener	6 (4 betas [boundary], drift, tau)	102.1	109.6
M2 Ex	Wiener	6 (4 betas [boundary], drift, tau)	71.7	71.3
M3(seq) Ex+LR	Wiener	7 (4 betas [boundary], alpha, drift, tau)	0 (reference)	0 (reference)
M3(Q) Ex=Q LR	Wiener	7 (4 betas [boundary], alpha, drift, tau)	63.3	61.6

inhibitory control accuracy, as measured by the proportion of successful Nogo inhibition. Results showed a significant positive effect of expectation on the subsequent inhibitory control accuracy (β_{a1} mean = 1.1, HDI = [0.17 1.98], p_{MCMC} = 0.012). To further demonstrate that subjects tend to compute expectation by calculating the specific sequence (Eq. 3) rather than using Q, we fitted a control model (see Methods, Model 4). This model included a θ parameter that reflects the rate at which subjects computed expectation using Eq. 3. As expected, the control model showed that the θ parameter was greater than 0.5 (mean = 0.77, HDI: [0.53 0.99], p_{MCMC} = 0.03), indicating that participants used the sequences of Go stimuli and the probability of Nogo to build their conflict expectation.

In summary, taking together results show that individuals adjust their RT according to the expectancy of the conflict stimuli—such processing, which could reflect cognitive control allocations, involves learning from past experiences in the environment.

GNG behavioral replication sample

We carried out a replication of the behavioral analysis in an independent sample of 57 participants. The task presented two modifications to control possible confounding factors. First, the sequences were not restricted to a maximum of seven Go stimuli, and the sequence formation was completely randomized following a 0.25 probability of Nogo occurrence (see Methods). This leads to the probability of each sequence decreasing with its length (see Methods). Notably, it has been proposed that the perception of a sequence of stimuli is influenced primarily by the timing of presentation rather than by task structure or the actual dependency between stimuli[40,46,47]. Thus, we expect that the build of expectation as a sequence of stimuli will be maintained regardless of the modification of the sequence. Second, the stimuli were letters (O and X) rather than colors to avoid possible color bias, and they were counterbalanced to serve as Go or NoGo stimuli in the two blocks for each subject. We replicated all the findings of the original sample (Supplementary Fig. 2). The early Go stimuli were faster (mean difference = −21 ms, CI = [−26, −15], Wilcoxon test, p = 7e-11, effect size r = 0.78), and the Nogo stimuli preceded by short Go sequences were less accurately inhibited (mean rate difference = 0.09, CI = [0.07, 0.11], Wilcoxon test, p = 1e-10, effect size r = 0.86). The M3 model with DDM fitted the data best, and the Ex regressor significantly differentiated from zero (β_1 Expectation mean = 51.7, 95% HDI: [51 62], p_{MCMC} < 0.001, see Supplementary Fig. 5). These results showed that expectation generation is a robust phenomenon, occurring despite modifications to the specific structure of the task (in this case, the specific length of the sequences) or stimulus saliency.

MRI experiment: modeling Multi-Source Interference Task (MSIT)

Our next objective was to identify the brain areas responsible for computing the expectation of conflict stimuli. We utilized the fMRI technique due to its high spatial resolution to achieve this goal. However, the slow dynamics of hemodynamic responses precluded using fast stimuli presentation tasks and, therefore, the generation of sequence effects, as seen in the GNG task[40]. To overcome this limitation, we designed a task and analysis based on the same rationale as the behavioral experiments adapted for fMRI. Specifically, we used the MSIT task, which involved variable sequences of congruent and incongruent stimuli, to obtain a balanced number of trials for the contrast (see Methods and Results sections below). Furthermore, for the analysis, we used conflict expectation as equivalent to the probability of conflict (i.e., Ex = Q, instead of Eq. 3, Model 3(Q), see Fig. 2A) as has been done in other research studies with large interstimulus intervals[39,45]. Since this variable updates on a trial-by-trial basis, we employed event-related analysis to evaluate these changes over time.

Following the preceding rationale, we tested whether subjects adjusted their reaction time according to the expectation of the occurrence of conflict stimuli. First, as in the behavioral experiment, we separated the first two stimuli in a sequence with the subsequent three stimuli (i.e., 1st and 2nd vs. 3rd, 4th, and 5th stimuli) in a sample of 26 participants. Following the behavioral model utilized in the GNG task, we expect that in the early trial for congruent sequences, subjects should expect more conflict than in the late trials, and vice versa for incongruent sequences. Accordingly, the trials with more predicted conflict expectation present slower RT (mean differences: 70.6 ms, CI = [85.9 55.3], p = 2.9e-8, effect size r = 0.87, Fig. 2C). Accuracy modulation was found only for incongruent sequences representing conflict stimuli (mean rate differences: 0.06, CI = [0.03 0.1], p = 0.0007, effect size r = 0.59). We then applied the M3(Q) model using the drift-diffusion model. The results showed that the probability of conflict significantly increases the RT in the MSIT task (β_1 Expectation mean = 1.07, HDI: [0.74 1.43], p_{MCMC} < 0.001, Fig. 2C, see Supplementary Table 3). As expected, conflict stimuli are slower than no conflict stimuli (β Conflict mean = 0.32, HDI: [0.22 0.41], p_{MCMC} < 0.001). Finally, we also fitted the other three models to test whether the proposed computation best fits the data. As predicted, the selected model presents the smallest DIC and LOOIC (see Supplementary Table 3). Accordingly, the control model M4 showed that the θ parameter was smaller than 0.5 (mean = 0.1, HDI: [1e-6, 0.29], p_{MCMC} = 0.01), indicating that subjects tend to compute expectation as equal to Q rather than calculating the specific sequence as in Eq. 3.

In summary, the MSIT task allows for the identification of homologous expectation processing, utilizing a computational mechanism similar to that specified in the GNG task. This computation involves learning from past stimuli to adjust cognitive control.

MRI experiment: brain activity correlating with expectancy of conflict

To evaluate the brain areas where activity correlated with the expectation of conflicting stimuli, we modeled the BOLD signal on a trial-by-trial basis, using both conflict expectation and the presentation of a conflicting or non-conflicting stimulus in the current trial. This analysis showed that the regressor of expectation (Ex) exhibited a significant correlation with bilateral activity in the superior frontal gyrus (SFG) (see Fig. 2C) and the medial parietal cortex (see Supplementary Table 4). Furthermore, the contrast between conflict and non-conflict stimuli presented a significant correlation with the activity in the frontal eye field and the inferior frontal junction (IFJ) in the lateral prefrontal cortex in both hemispheres, as well as other brain areas (see Fig. 2C and Supplementary Table 4).

MSIT replication sample

We carried out a replication of the behavioral and fMRI analysis in an independent sample of 56 subjects. We replicated all behavioral findings of the original sample (Supplementary Fig. 6). The trials with predicted less conflict expectation within a sequence were faster for

https://doi.org/10.1038/s41467-024-54244-8

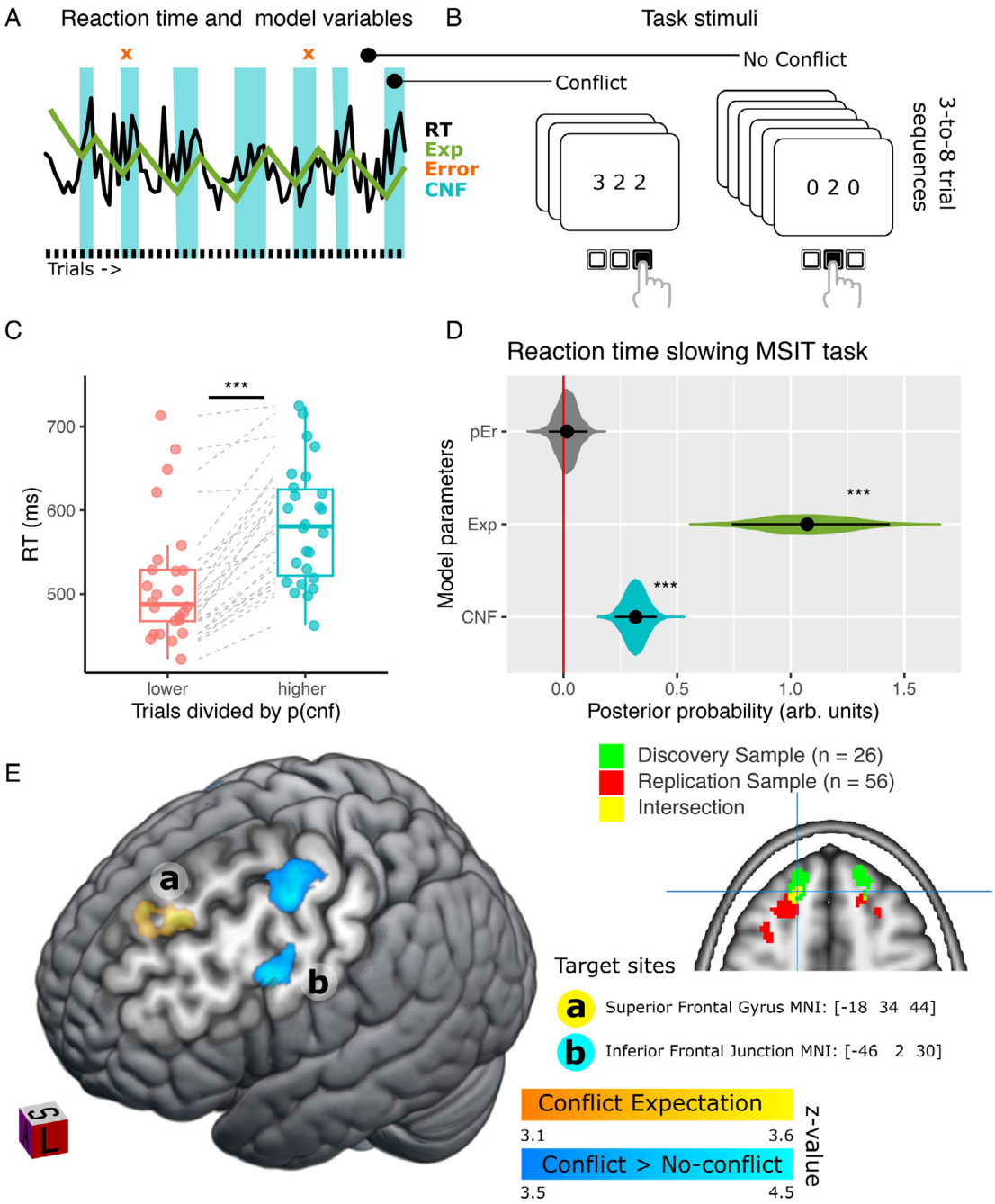

Fig. 2 | MRI experiment results. A Example of trial-by-trial variation in the reaction time and model variables. **B** MSIT Task stimuli. **C** Comparison of reaction times between trials with predicted lower and higher conflict expectations per sequence ($n = 26$ participants, Wilcoxon test, two-sided, $p = 2.9e\text{-}8$). Boxplots display the extreme values, interquartile range, and median, and each point representing the mean for an individual subject. **D** Posterior distribution of model parameters ($n = 26$ participants, Bayesian hypothesis test using p_{MCMC}, two-sided, $p < 0.001$). Black dots represent the mean of the distribution, and black lines represent the 95% high-density intervals. The colored areas represent the complete posterior distribution. **E** Brain activity is associated with conflict expectation in the lateral prefrontal cortex (yellow) and conflict stimulus processing (blue). Lowercase letters a and b indicate the target sites for TMS experiments. The right panel shows the comparative results for the Conflict Expectancy regressor for the discovery sample (red) and the replication sample (green), highlighting the intersection of both results (yellow). The blue lines indicate the site of TMS stimulation in the SFG. * indicates $p < 0.05$, ** $p < 0.01$,*** $p < 0.001$. CNF conflict trial, Ex conflict expectation, MSIT multiple source interference task, pEr error in the prior trial, p(cnf) predicted probability of conflict, RT reaction time, SFG superior frontal gyrus, TMS transcranial magnetic stimulation. See Supplementary Tables 3 and 4. Source data are provided as a SourceData file.

both sequences (mean difference = −55 ms, CI = [−66 −43], Wilcoxon test, $p = 1e\text{-}10$, effect size $r = 0.86$), and less accurate for incongruent sequences only (mean rate difference = 0.05, CI = [0.02 0.07], Wilcoxon test, $p = 0.001$, effect size $r = 0.42$). The Expectation regressor significantly differentiated from zero (posterior distribution, β_1 Expectation mean = 1.08, HDI: [0.77 1.36], $p_{MCMC} < 0.001$, Supplementary Fig. 6). fMRI results also showed a bilateral activity in the superior frontal gyrus for the Expectation regressor, as illustrated in the overlaping area shown in the right panel of Fig. 2E, as well as the intersection area in the medial parietal cortex.

https://doi.org/10.1038/s41467-024-54244-8

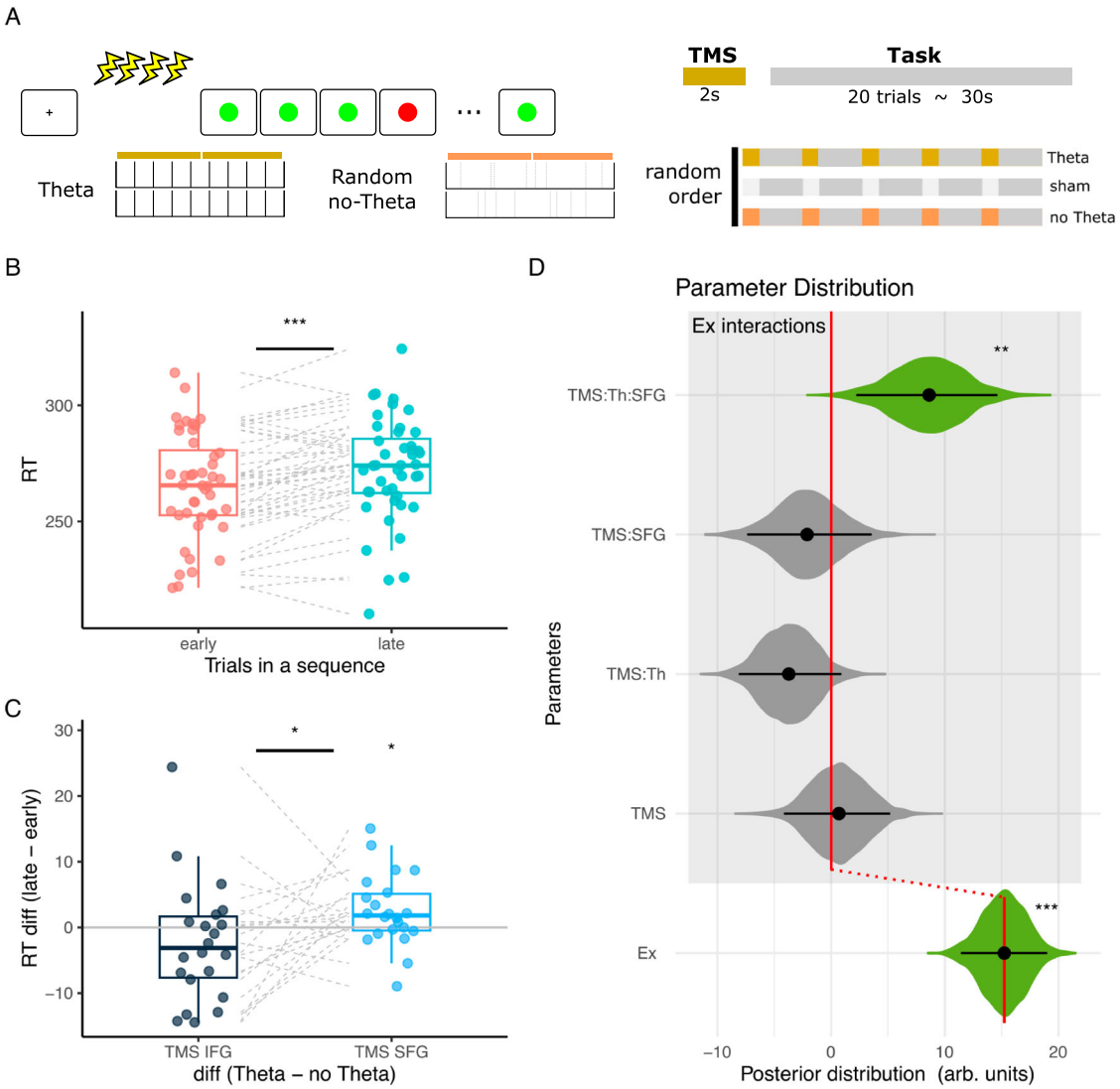

Fig. 3 | TMS experiment behavioral results. A Experimental design of the Go-Nogo Task during EEG-TMS sessions. **B** Reaction time (RT) modulation by the trial position in a sequence ($n = 44$ sessions, Wilcoxon test, two-sided, $p = 0.0001$). **C** The modulation of the effect of trial position by the TMS stimulation ($n = 22$ participants, Wilcoxon test, two-sided, TMS-SFG $p = 0.04$, TMS-SFG vs TMS-IFG $p = 0.04$, uncorrected). **B**, **C** Boxplots display the extreme values, interquartile range, and median, and each point representing the mean for an individual subject. **D** Posterior distribution of model parameters ($n = 24$ participants, Bayesian hypothesis test using p_{MCMC}, two-sided, Ex $p_{MCMC} < 0.001$, Ex:TMS:Th:SFG interaction $p_{MCMC} = 0.0006$). Black dots represent the mean of the distribution, and black lines represent the 95% high-density intervals. The colored areas represent the complete posterior distribution. The grey rectangle indicates interaction regressors with the Ex regressor. * indicates $p < 0.05$, ** $p < 0.01$, *** $p < 0.001$. RT reaction time, SFG superior frontal gyrus, Th theta rhythm, TMS transcranial magnetic stimulation. see Supplementary Table 5. Source data are provided as a SourceData file.

EEG-TMS experiment

SFG TMS at theta frequency enhances conflict expectation during the GNG Task. Prior work has demonstrated that theta oscillation and lateral prefrontal cortex activity correlate with proactive cognitive control[7,14,48]. Hence, based on our fMRI results, we aimed to investigate the causal relationship between theta activity in the SFG and the conflict expectation. To this end, we conducted a TMS-EEG experiment using TMS stimulation before each 20-stimuli run of the GNG task (Fig. 3A). We selected a 5 Hz frequency for stimulation and used arrhythmic TMS and sham stimulation as control. Considering our fMRI results, we stimulated two different areas, the left SFG (MNI: [−18 34 44], peak coordinate for the Expectation regressor, see Fig. 2) and the left IFJ (MNI: [−46 2 30], peak coordinate for the Conflict regressor, see Fig. 2), in separate sessions to assess their respective involvement. We selected the left hemisphere because we found that the peak of activity was located in this region. Additionally, patients with altered conflict expectation processing exhibited decreased theta activity that was left-lateralized[7]. However, there is no clear evidence to suggest that the computations themselves are lateralized. Thus, we targeted the left SFG to investigate its role in the conflict expectation while controlling for potential effects on inhibitory control by stimulating the IFJ[49,50].

Using the peak activity in the SFG as our target site, we explored the causal relationship between theta activity and the conflict expectation. Our behavioral results revealed that participants exhibited slower RT as the conflict expectation increased. The late trials of a sequence (the 3rd, 4th, and 5th stimuli;) were slower than early trials (the 1st and 2nd stimuli, contrast late - early trails, mean difference 7.1 ms, CI = [4 10.2], median = 7.6; Wilcoxon test $p = 0.0001$, $n = 44$, $r = 0.57$, Fig. 3B). This effect was significantly greater as the theta TMS stimulation was applied in the SFG in comparison with arrhythmic TMS stimulation (mean difference = 2.5 ms, CI = [0.08 4.9], median = 1.8, Wilcoxon test $p = 0.04$, $r = 0.43$, $n = 22$, Fig. 3C). No effect was found when theta TMS stimulation was applied in the IFJ (mean differences:

https://doi.org/10.1038/s41467-024-54244-8

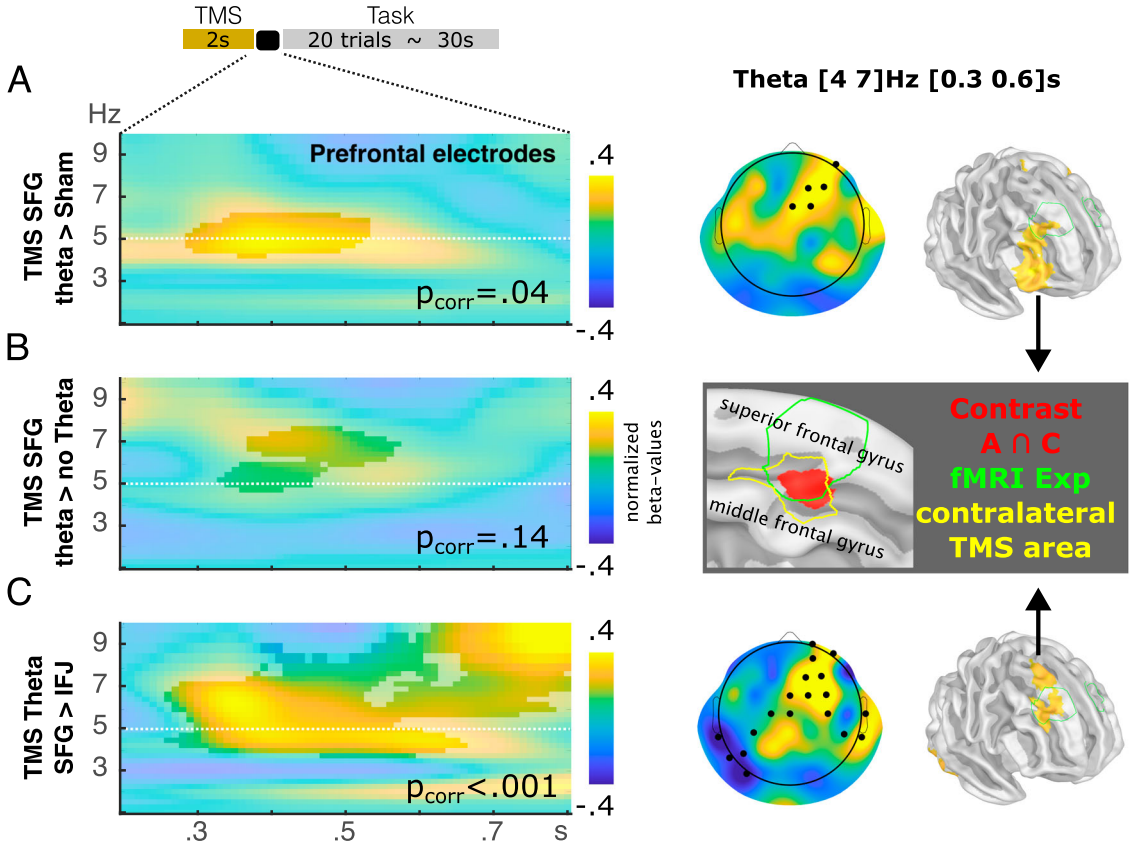

Fig. 4 | Oscillatory effects post-TMS. A Power increases after theta TMS stimulation over the SFG compared to sham stimulation. The left panel shows the time-frequency chart for a second after the last TMS pulse and before the first Go stimuli (TMS_{theta} regressor for SFG sessions) over frontal electrodes (F1, F2, F3, F4, Fz, FC1, FC2, FC3, FC4 and FCz). The right panel shows the scalp distribution and source estimation of theta modulation. **B** Power increases after theta TMS stimulation over the SFG compared to no theta stimulation (TMS_{theta} regressor > $TMS_{no\text{-}theta}$ regressor for SFG sessions). No modulation in source space survived multiple comparison corrections. **C** Power increases after theta TMS stimulation over the SFG compared to theta TMS stimulation over the IFJ (TMS_{theta} regressor for SFG sessions > TMS_{theta} regressor for IFJ sessions). The scalp distribution and source estimation reveal the main modulation of the left lateral frontal cortex. The gray rectangle shows the conjunction analysis for the contrasts shown in (**A**) and (**B**). The green line represents the BOLD modulation for the Ex regressor in fMRI experiments (see Fig. 2). The yellow line represents the homologous contralateral area of stimulation (Braintomme atlas area: A9/46d[98]). **A**–**C** The highlighted areas represent significant modulation identified by the cluster-based permutation test (two-side test, corrected by multiple comparison). The *p*-value indicated in each chart represents the highest $p_{corrected}$ value of the cluster highlighted for that chart. The electrodes highlighted indicate those with significant modulation. IFJ inferior frontal junction, SFG superior frontal gyrus, TMS transcranial magnetic stimulation. Source data are provided as a SourceData file.

−2.2 ms, CI = [−6 1.7], median = −3.1, Wilcoxon test $p = 0.2$, $r = 0.2$, $n = 22$, Fig. 3C). Thus, the theta effect was significantly greater for the SFG than for the IFJ TMS stimulation (mean differences = 4.8 ms, CI = [0.2 9.4], Wilcoxon test $p = 0.04$, $r = 0.44$, $n = 22$, Fig. 3C).

We then tested the cognitive model M3, showing the same effect. Specifically, we found that participants during sham stimulation in both sessions showed similar behavior to those in the behavioral experiment, increasing their reaction time in response to the conflict expectation (β_1 Ex mean: 14.3, HDI: [10.3, 18.3], $p_{MCMC} < 0.001$, see Supplementary Table 5). Regarding TMS stimulation, we observed that the main effect of TMS, regardless of its frequency or target site, did not significantly impact participants' RT (β_8 TMS mean: 0.4, HDI: [−2.4, 3.0], $p_{MCMC} = 0.76$; β_4 Ex*TMS mean: 1.52, HDI: [−3.5 6.5], $p_{MCMC} = 0.56$). However, we found that theta stimulation over the SFG specifically resulted in an expectation-related increase in RT. This was evidenced by a significant interaction between expectation, TMS, theta, and the SFG (β_7 $Ex*TMS_{theta*SFG}$ mean = 9.3, HDI = [3.5 16.3], $p_{MCMC} = 0.0006$; Cohen'd mean = 0.83, HDI = [0.65 1.0], see Supplementary Table 5 and Fig. 3B). Concerning the accuracy, the TMS stimulation had no direct effect on the accuracy (β_{11a} TMS_{SFG} mean = 0.042, HDI = [−0.25 0.34], $p_{MCMC} = 0.7$). However, we did observe that the impact of expectation given by $TMS_{theta*SFG}$ stimulation increase the accuracy of following Nogo stimuli (β_{a7} $Ex*TMS_{theta*SFG}$ mean = 0.27, HDI = [0.05 0.49], $p_{MCMC} = 0.002$; β_{1a} Ex: mean = 0.44 HDI = [0.19 0.68], $p_{MCMC} < 0.001$). The findings suggest that theta stimulation over the SFG may precisely modulate cognitive processes related to conflict expectation.

TMS stimulation in the SFG increases endogenous theta oscillation. We conducted a power analysis of the EEG signal to assess whether TMS theta stimulation induces oscillatory brain activity. For each session, we carried out a general linear model using condition as a regressor in a first-level analysis, and then tested the consistency between subjects using a second-level analysis (see Methods). We examined the time windows following TMS stimulation and just before task stimulus presentation, revealing a specific effect of TMS stimulation. Rhythmic theta stimulation over the SFG significantly enhanced theta activity compared to sham stimulation (Fig. 4A). We found the same tendency compared to arrhythmic stimulation, but the effect did not survive cluster correction (Fig. 4B). We also observed higher theta activity than theta stimulation over the IFJ (Fig. 4C). Source analysis indicated the involvement of the right lateral prefrontal cortex. The gray rectangle in Fig. 4 represents the common area revealed by conjunction analyses, as observed in the contrasts Theta TMS > sham

in SFG and Theta TMS in SFG > Theta TMS in IFJ. Notably, a shared modulation was identified in a cortical region where we had observed modulation in the fMRI experiment, representing the contralateral stimulation area. Overall, TMS theta stimulation can generate brain oscillatory activity in the theta range contralateral to the stimulated brain region in the SFG.

The conflict expectation modulates the amplitude and the phase-amplitude coupling of the lateral frontal oscillatory activity. We next analyzed the brain activity during task execution. We conducted a power analysis of the electrophysiological recordings and correlated it with the conflict expectation predicted by the behavioral model. These analyses indicated a statistically significant modulation in theta activity associated with the conflict expectation. During the sham conditions, a post-stimulus modulation in theta oscillations related to conflict expectation was observed at the frontal electrodes in response to the Go stimulus (see Fig. 5A). Source analysis revealed that this modulation was localized in the right lateral prefrontal region. Previous evidence suggests prefrontal areas exert control functions through phase-amplitude coupling (PAC)[51]. For instance, studies have demonstrated that the low-frequency phase in the delta/theta range modulates the amplitude of alpha/beta oscillations, reflecting control signals over other cortical regions, such as motor and premotor areas[52–54]. Hence, we assessed PAC modulation that could reflect increased control associated with heightened expectation of conflict. We calculated the Envelope-to-Signal correlation in a time window following stimulus presentation and correlated this with the expectative of conflict stimuli. This analysis revealed that the expectative of conflict correlated with an increased PAC between delta/theta and alpha/beta oscillations (Fig. 5B). This modulation was placed over the right central electrodes that were compatible with the motor and premotor areas.

TMS stimulation modulates theta oscillations in lateral prefrontal regions related to the conflict expectation. Next, we explore TMS's modulation in electrophysiological activity related to conflict expectations. Exploring the interaction among Expectation, TMS, and theta stimulation, we found a positive modulation in frontolateral electrodes for both theta and alpha oscillations generated by TMS over SFG (Fig. 5C). Contrasting the preceding interaction between the SFG and IFJ TMS, a similar modulation was detected involving theta and alpha oscillations (Fig. 5D). Scalp topographies and source analysis of this modulation reveal the prominent participation of alpha modulation in the right frontolateral region involving premotor and motor areas and the parietal region. No modulation was found to TMS in the correlation between PAC modulation and conflict expectations.

Discussion

Improving our understanding of anticipation and adaptation to conflict stimuli is pivotal for implementing therapies targeting such processing across diverse neuropsychiatric disorders. Employing an integrative methodology that combines computational modeling, neuroimaging, transcranial magnetic stimulation, and electroencephalography, our goal was to uncover the mechanisms underlying these cognitive processes. Our results contribute to establishing the computational and neurobiological mechanisms underlying the formation of expectations related to conflicting events, alongside the causal involvement of theta oscillations in the lateral prefrontal cortex.

Our behavioral modeling revealed that participants adapt their reaction times in anticipation of conflict stimuli, as evidenced by slower responses following a higher expectation of such events. This adaptive behavior suggests a flexible mechanism wherein individuals dynamically allocate cognitive resources based on learned expectations[55,56]. Our task variations were designed to investigate the factors influencing expectation formation and to identify the core components of the computational processes underlying this formation. Across tasks and replication samples, models incorporating learning provided the best fit to the data, consistently computing the probability of conflict based on context. This probability can be used directly or mediated by additional processing to calculate sequence probability and build expectations. Thus, expectation effects involve the anticipatory engagement of cognitive control mechanisms, while the more commonly studied adaptation effect, known as the Gratton effect, may involve the strengthening of task representations or the adjustment of control settings in a reactive manner[41,42]. Recent research indicates that the dynamic process of learning from conflicting stimuli in the environment is correlated to multidimensional representations within neuronal ensembles[45]. Furthermore, indicators of conflict occurrence may be associated with accumulating learning from conflicts over time, influencing future responses to similar conflicting stimuli[45,57]. Interestingly, this learning has specific task-dependent and general domain mechanisms[45]. Our cognitive model posits analogous patterns, indicating the existence of a domain-general computation that remains consistent across tasks and adapts to learn from conflicting environmental stimuli. Conversely, specific expectations, like the sequence effect, undergo adaptation tailored to the particular demands of the task, such as adjusting to interstimulus intervals[40]. Hence, the cognitive computation model proposed here can be understood as a general domain processing that could occur in different situations and be utilized in various ways depending on the specific context and demands. Thus, this computational process can be tested in different contexts and has the potential to reconcile contradictory evidence and theoretical propositions to understand conflict adaptation and flexible cognitive control[26,27], especially concerning understanding various neuropsychiatric pathologies[58].

Our fMRI results further elucidated the relationship between conflict expectation and frontal activity. The observed engagement of distinct regions within the lateral prefrontal cortex in response to conflict stimuli and conflict probability is consistent with prior neuroimaging research, which has consistently shown the frontal brain areas' involvement in conflict resolution, conflict monitoring, cognitive control, and response inhibition[2,30,59,60]. In the study of perceptual decision-making, a dissociation between various regions of the lateral prefrontal cortex has been linked to distinct cognitive computations[61,62]. Our results highlight the differential causal role of the SFG and IFJ in mediating the impact of conflict expectation on behavioral performance. The SFG is a region implicated in different tasks, including integrating working memory and inhibitory control to solve cognitive tasks[63] and accumulating and valuing sensory evidence from the environment[62]. Moreover, alteration in SFG activity is associated with disorders such as bipolar depression[9] and schizophrenia[12,13]. On the other hand, the IFJ is essential for executive functions[64] like control of action, attention, and memory[65], and its bilateral lesion causes the dysexecutive syndrome[64]. Interestingly, the interaction between these two areas is related to the flexible use of proactive or reactive strategy[66]. Thus, the lateral frontal areas and their associated networks play a crucial role in abstracting diverse environmental features to estimate the probability of encountering difficult situations. This process involves computations akin to learning algorithms that dynamically adjust real-time control mechanisms to adapt behavior.

Our EEG-TMS results shed light on the neurobiological implementation of the described computational mechanism. TMS stimulation targeting the left SFG at theta frequency enhances conflict expectation during the GNG task. Using repetitive TMS to increase cortical excitability, a study showed that stimulation of the left lateral prefrontal cortex, rather than the right, enhances proactive cognitive control[67]. In addition, evidence has shown that using TMS with specific experimental designs has improved other functions such as verbal memory[68] and working memory[69,70]. Although TMS over the left frontal cortex has been proposed to enhance frontal functions such as

https://doi.org/10.1038/s41467-024-54244-8

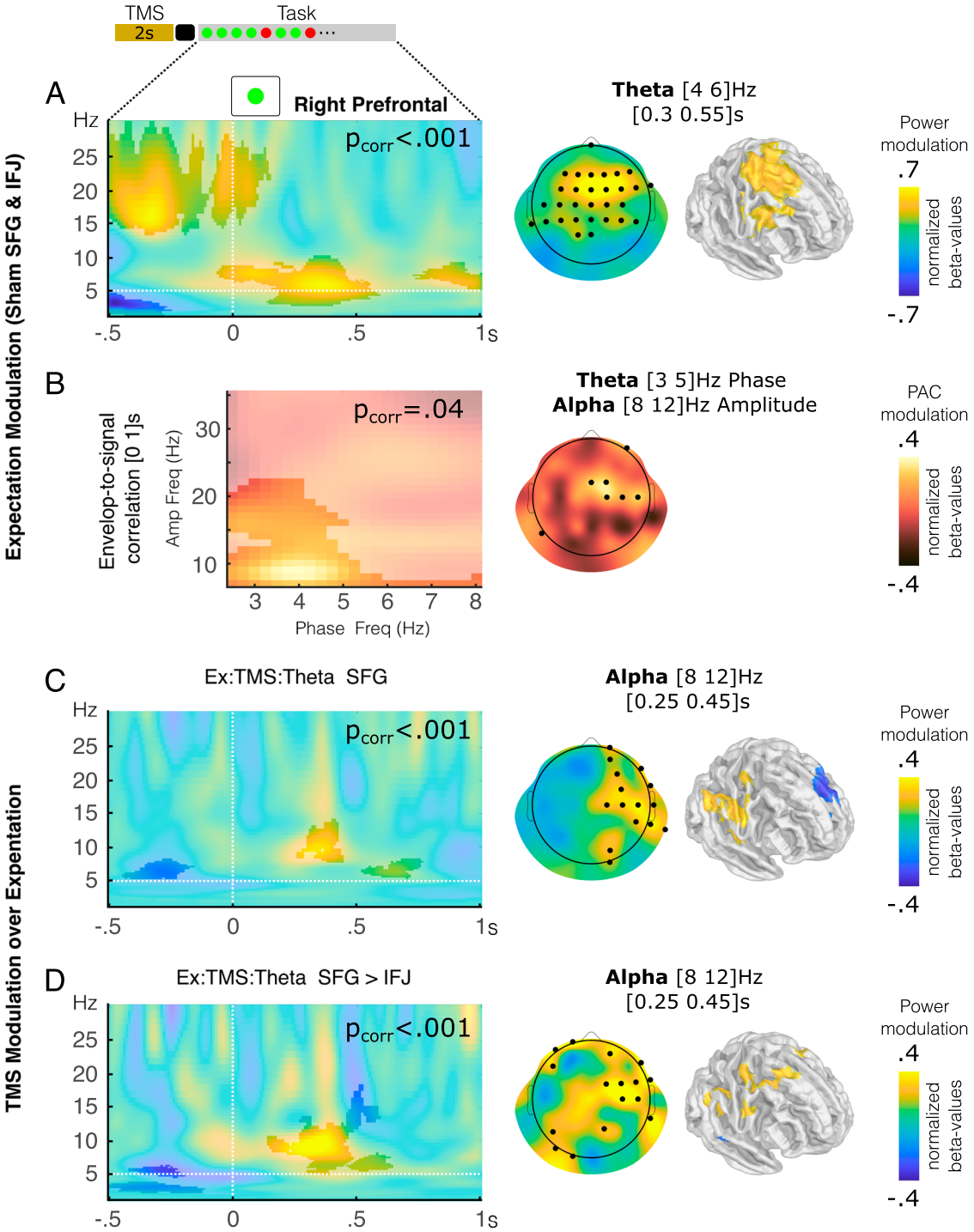

Fig. 5 | Oscillatory modulation related to conflict expectation and TMS effects. **A** Oscillatory activity associated with the expectation of conflict in sham conditions is depicted (Ex regressor for SFG and IFJ sessions). The left panel illustrates the time-frequency chart over frontal electrodes (F1, F2, F3, F4, Fz, FC1, FC2, FC3, FC4 and FCz), while the right panel displays the topographic and cortical surface distribution of theta modulation. **B** Phase amplitude coupling during the second following Go stimuli modulated by the expectation of control (Ex regressor for SFG and IFJ sessions). **C** Oscillatory activity related to the conflict expectation and TMS theta interaction during SFG stimulation ($Ex*TMS_{theta}$ regressor for SFG). **D** Oscillatory activity related to the conflict expectation and TMS theta interaction for the contrast between the SFG and IFJ stimulation ($Ex*TMS_{theta}$ regressor for SFG > $Ex*TMS_{theta}$ regressor for IFJ). **A**–**D** The highlighted areas represent significant modulation identified by the cluster-based permutation test (two-side test, corrected by multiple comparison). The *p*-value indicated in each chart represents the highest $p_{corrected}$ value of the cluster highlighted for that chart. The electrodes highlighted indicate those with significant modulation. The vertical dotted lines denote the appearance of Go stimuli, and the horizontal dotted line represents the frequency of theta stimulation. IFJ inferior frontal junction, SFG superior frontal gyrus, TMS transcranial magnetic stimulation. Source data are provided as a SourceData file.

flexibility and conflict adaptation, contradictory results exist[71]. The variability in outcomes observed in studies concerning the stimulation of the left lateral prefrontal cortex may stem from a deficiency in precise computational mechanisms governing cognitive processes and the inability to target specific neuronal activities accurately. Our experimental approach enabled us to intervene more precisely the underlying neurobiological sources linking brain function and behavior. Previous research has shown that TMS can induce theta activity during task execution[69]. In line with these observations, we found an increase in theta activity following TMS stimuli, demonstrating that exogenous stimulation with TMS can interfere with and augment endogenous oscillatory activity[72]. Although we did not conduct specific analyses to determine whether theta modulation met the criteria for persistent oscillations, evidence from neural models and empirical data suggests that prefrontal theta activity represents a persistent oscillatory phenomenon in the context of cognitive control[73].

Taken together, our results indicate a specific computational role for theta oscillations that involves learning from the environment and forming sequences of stimuli dependent on task demands. Interestingly, this mechanism may help reconcile contradictory effects described in the conflict adaptation literature[27]. For example, in tasks with rapid stimulus presentation, longer sequences of non-conflict stimuli initially increase cognitive control but subsequently decrease it, reflecting the dynamics of anticipation effects. Another relevant issue for further research is the variation of inter-stimulus intervals within the same task. Our control model (M4) could be integrated more comprehensively to account for how longer inter-stimulus intervals affect sequence building without impacting the learning of conflict probabilities, thereby influencing the expectation of conflict. Interestingly, evidence integrating neural models with electrophysiological recordings suggests that theta oscillations can vary in peak frequency to accommodate task demands[73]. Thus, the length of the theta cycle may help explain how computations of sequences or events are carried out by neural systems and how these computations are influenced by inter-stimulus intervals[73].

EEG source analyses of the oscillation induced by TMS shows contralateral activity. This activity could be explained by the fact that TMS does not have a local effect but a network effect[74,75]. This non-local effect depends on structural rather than functional connectivity[76]. Stimulation with TMS in one area generated secondary stimulation in its connected areas, demonstrating an effect in its homologous contralateral area, as seen in studies with TMS in parietal regions[77], in the auditory cortex[78], and in the motor cortex[79]. This can be explained by the fact that TMS depolarizes cortical neurons, and the activity expands to all connected areas. This effect of TMS could serve the basis for rehabilitation therapies[80], allowing the application of non-invasive interventions at the cortical level, producing an effect in deeper areas[81]. In this context, it is relevant to consider individual differences in functional brain connectivity, which could interfere with the effects of TMS[82]. Additionally, at the site of direct stimulation, the depolarization of different types of neurons in the local circuit generates a non-physiological functioning that may explain unclear effects on activity observed in some research at the target site[83]. However, in the connected area, the stimulation induced by the depolarization of pyramidal neurons at the target site can yield a more physiological stimulation of the output circuit, which can explain the activity and entrainment of oscillatory theta activity found in the contralateral area in our experiment.

Frontal theta activity has been related to diverse cognitive functions, including conflict evaluation and monitoring. Our results indicated that the conflict expectation modulates the power of theta activity in the right lateral prefrontal cortex according to the cognitive demands of the task. As a complex mechanism, cognitive control involves theta oscillations and the increase of theta gamma PAC in the dorsomedial and dorsolateral prefrontal cortex[84] and the orbitofrontal cortex[85]. Hence, our cross-frequency analysis indicates that conflict expectation is also related to an increased PAC between the phase of delta/theta and the amplitude of alpha/beta oscillations. The later modulation could be the mechanism by which cognitive control is exerted towards the motor and premotor cortex[52], relating to inhibitory control[54]. Additionally, delta-beta coupling has been proposed as a marker for anticipatory anxiety in pathologies such as social anxiety disorder[86]. Interestingly, TMS modulates theta and alpha activity in the lateral prefrontal cortex during task execution, increasing conflict expectations' behavioral effect. The results show that these oscillations are a key component of algorithmic processing to face conflict tasks, as has been demonstrated and postulated in other cognitive processes such as the attentional network[87] and working memory[88]. The contrast between TMS stimulation at theta rhythm in different regions of the lateral prefrontal cortex further demonstrates the specificity of the SFG in this computational process. Hence, considering all EEG results, the theta and alpha oscillations in a prefrontal network could be the mechanism by which the computation of conflict expectation is implemented in the brain.

Alterations in the expectancy of conflict events have been associated with neuropsychiatric disorders that profoundly impact the quality of life for many individuals. Our results describe a cognitive computation underlying conflict expectation and its causal neurobiological mechanism involving theta activity in the SFG. Given the development of diverse techniques for intervening in brain activity in a non-invasive manner in clinical settings[89] and the known alteration of brain oscillation in diverse disorders[7,34,48,90,91], unraveling this mechanism holds promise for developing interventions to address these cognitive alterations in neuropsychiatric disorders, thereby enhancing overall cognitive function and quality of life.

Methods

Participants

One hundred seventy-five healthy subjects participated in this research. All participants gave their informed consent, and all experimental procedures were approved by the Ethics Committee of Clinica Alemana - Universidad del Desarrollo, Chile (Folios 2018-03 and 2020-67). The research consisted of 214 experiential sessions, structured as follows. In the first experiment, 30 subjects (15 women, ages ranging between 18 and 20 years) participated in the behavioral session and 57 in the replication sample (32 women, ages ranging between 23 and 60 years). In the subsequent experiments, another sample of subjects participated as follows. In the second experiment, 26 subjects (15 women, ages ranging between 18 and 35 years) participated in the fMRI session and 56 in the replication sample (29 women, ages ranging between 18 and 37 years); in the third experiment, 24 subjects (13 women, ages ranging between 18 and 35 years) participated in the EEG-TMS sessions. A total of 18 subjects participated in experiments 2 and 3. All participants gave informed consent. Experiments were conducted in the Social Neuroscience and Neuromodulation Laboratory at the Centro de Investigación en Complejidad Social (neuroCICS) at the Universidad del Desarrollo and the Unidad de Imágenes Cuantitativas Avanzadas (UNICA) at the Clínica Alemana de Santiago.

Experimental design

For the behavioral experiment, subjects participated in the GNG task. With these data, different behavioral models were tested to explain conflict expectancy and variations in reaction time. The best-fitted model was used to analyze the data from experiments 2 and 3 (Fig. 1 and Supplementary Fig. 1). For the second experiment, subjects participated in an MRI session and solved the MSIT task. Imaging data were analyzed by integrating regressors from behavioral modeling of the MSIT task to identify target sites for experiment 3. In the third experiment, subjects participated in two sessions of TMS-EEG (Supplementary Fig. 1) while they performed the GNG task. In one session,

the stimulation was delivered over the superior frontal gyrus (SFG); in the other, it was in the IFJ. The stimulation site for each session was randomized, and the sessions were balanced.

Tasks

Go-Nogo Task. During the behavioral and TMS-EEG experiments, participants completed the Go-Nogo task, which involved viewing green or red stimuli on a screen. Participants were instructed to press a keypad button for the green stimuli (Go stimulus) but not to press the button for the red stimuli (Nogo stimulus). In the behavioral experiments, participants completed two blocks, each consisting of 150 trials (Fig. 1). In the TMS-EEG sessions (experiment 3), participants completed four blocks containing three sub-blocks of 100 stimuli. The stimuli were separated into five runs of 20 stimuli each. Before each 20-stimuli run, 10 TMS pulse series were applied for 2 s in different patterns: rhythmic (5 Hz), arrhythmic, or sham (Fig. 3). The behavioral results of the GNG task were analyzed by fitting different models to estimate the probability of conflict and the expectation of conflict occurrence. Each stimulus was presented over 300 ms, and the interstimulus interval varied between 900 and 1400 ms. The occurrence of Nogo stimuli was set to 0.25, interspersed within sequences ranging from 1 to 7 Go stimuli. This task structure ensured that all sequences were presented with similar frequencies, ~0.14.

Go-Nogo Task for Replication Sample. Following the same rationale as the previous task, for the replication sample, the Go-Nogo task was presented in two blocks of 150 trials where the stimuli were letters (X or O). They were randomly assigned and counterbalanced so that each participant encountered a letter representing the Go stimulus in one block and the Nogo stimulus in the other block, and vice versa. Each stimulus was presented over 300 ms, and the interstimulus interval varied between 900 and 1400 ms. The occurrence of Nogo stimuli was set to 0.25, and the length of the sequences of Go stimuli was not restricted. Thus, the frequency of sequences was different to the first task, ranging from seq=1 p ~ 0.18 to seq>7 p ~ 0.1.

MSIT task. During the MRI experiment, participants were presented with a set of stimuli consisting of three numbers and were asked to identify the number that was different from the other two using a keypad. The task included congruent and incongruent trial sequences of variable duration (3 to 8 trials). During congruent trial sequences, the different number matched its position on the keypad and was flanked by non-task-relevant numbers (zeros). In incongruent trial sequences, which were associated with great difficulty, the different numbers and their positions did not match, and the other numbers were task-relevant (Fig. 2). The occurrence of conflict stimuli was 0.5. Each stimulus was presented for 1000 ms, and the interstimulus interval varied between 1500 and 3000 ms.

Behavioral analysis

Behavioral analysis was conducted using a Hierarchical Bayesian approach, which leverages the aggregated information from the entire population sample to inform and constrain the parameter estimates for each individual. This approach incorporated two levels of random variation: the trial level (i) and the participant level (s). Models were compared using the Deviance Information Criterion (DIC) and the Leave-One-Out Information Criterion (LOOIC). All the models were fitted to the reaction times (RT) and were adjusted using R and JAGS software. For the Go-Nogo task, we tested two distributions: a log-normal and a Wiener process (DDM). Since for this task, for Go stimuli, there is only one correct response, and for incorrect ones, there is no response time, it is possible to compare these two distributions by fitting the model to correct Go stimuli only. Note that other studies have compared that this approach leads to a comparable model adjustment than that of dual response tasks[92]. Given its proposed influence on the speed-accuracy tradeoff that underlies cognitive control[93], we assumed that all regressors would affect the decision boundary (threshold) parameter, and we set the bias parameter to 0.5 (since it is not possible to adjust these parameters when there is no incorrect response time). Thus, for all models tested, we used the following equation:

$$RT \sim Weiner(boundary, drift, tau, bias) \tag{5}$$

where boundary were derived from the specific models (Eqs. 1 to 4). Additionally, to test the impact of expectation in accuracy, we constrained the model to include reaction time in the current trial (t) and accuracy (Acu) of the subsequent Nogo trial ($t+1$, where applicable) as follows.

$$Acu_{t+1} \sim Bernulli(logit^{-1}(rate_{t+1})) \tag{6}$$

$$CC_t = \beta_1 E_x + \beta_2 pCE + \beta_3 pOE \tag{7}$$

$$boundary_t = \beta_0 + CC_t \tag{8}$$

$$rate_{t+1} = \beta_{a0} + \beta_{a1} CC_t \tag{9}$$

For the preceding Eqs. (5 to 9), drift, tau, and all β represent free parameters. Note that the equation that affects the boundary is equal to the M3 model, with the only difference being that the intercept (β_0) is represented separately in order to obtain an independent intercept for Accuracy data (β_{a0}). In such a context, the influence of expectation on accuracy is represented by $\beta_{a1} * \beta_1$.

In the TMS-EEG experiment, we used the following equation to test the effect of TMS on expectancy.

$$\begin{aligned} boundary_t = {} & \beta_0 + \beta_1 Ex_t + \beta_2 pCE_t + \beta_3 pOE_t + \beta_4 Ex * TMS + \beta_5 Ex_t * TMS_{theta} \\ & + \beta_6 Ex_t * TMS_{sfg} + \beta_7 Ex_t * TMS_{sfg*theta} + \beta_8 TMS + \beta_9 TMS_{theta} \\ & + \beta_{10} TMS_{sfg} + \beta_{11} TMS_{theta*sfg} \end{aligned} \tag{10}$$

Where TMS represents the main effect of TMS stimulation, TMS_{theta} represents the effect of theta rhythmic stimulation, TMS_{sfg} the stimulation in SF, and $TMS_{theta*sfg}$ represents the specific effect of theta stimulation over SFG. Finally, in a similar way to the behavioral experiment, to evaluate whether TMS impacted accuracy by means of changes in expectancy, we constrained the model to include reaction time in the current trial (t) and accuracy (Acu) of the Nogo stimulus in the subsequent trial (where applicable) as follows.

$$\begin{aligned} CC_t = {} & \beta_1 Ex + \beta_2 pCE + \beta_3 pOE + \beta_4 Ex * TMS + \beta_5 Ex * TMS_{theta} \\ & + \beta_6 Ex * TMS_{sfg} + \beta_7 Ex * TMS_{sfg*theta} \end{aligned} \tag{11}$$

$$boundary_t = \beta_0 + CC_t + \beta_8 TMS + \beta_9 TMS_{theta} + \beta_{10} TMS_{sfg} + \beta_{11} TMS_{theta*sfg} \tag{12}$$

$$rate_{t+1} = \beta_{a0} + \beta_{a1} CC_t + \beta_{a2} TMS + \beta_{a3} TMS_{theta} + \beta_{a4} TMS_{sfg} + \beta_{a5} TMS_{theta*sfg} \tag{13}$$

All β parameters were parameterized using normal distributions, while the α parameter (learning rate, Eq. 4) was parameterized using a beta distribution. At the participant level, the model parameters were constrained by group-level hyperparameters. We assumed flat distributions for each parameter at the highest level of the hierarchy (hyperparameters).

We used the Gibbs sampler and Markov Chain Monte Carlo technique to perform posterior inference on the parameters in our Hierarchical Bayesian models. To ensure convergence, we drew a minimum of 2000 samples from an initial burn-in sequence, followed by 5000 new samples using three chains generated from different random number generators with different seeds. We thinned the resulting sample by a factor of 5 to reduce autocorrelation among the final samples for each parameter, resulting in a final set of 3000 samples. Gelman–Rubin tests confirmed the convergence of all latent variables in our models, with a statistic near 1 indicating convergence to the target posterior distribution. Due to computational capacity limitations when applying this approach to large experiments with complex models, in the TMS-EEG experiment, we estimated individual alpha parameters using 20% of the data (specifically, the fifth run of each sub-block). We then used these individual alpha parameters to estimate the remaining parameters using the complete data series. Similar approaches have been used in prior studies, yielding consistent results[45,94].

Control model

To test the differences in expectation computation due to the longer interstimulus interval of the MSIT task, we fitted a control model, M5. In this model, subjects compute Ex using Eq. 3 if a variable $A = 1$, and Ex = Q if $A = 0$. The variable A is generated by a Bernoulli process as follows:

$$A \sim \text{Bernulli}(\theta) \tag{14}$$

Where θ is a free parameter that reflects the population rate of subjects using the computation proposed in Eq. 3.

Anatomical data

All participants in experiments 2 and 3 underwent a 3D anatomical MPRAGE T1-weighted (repetition time [TR]/ echo time [TE] = 2530/2.19 ms, inversion time [TI] = 1100 ms, flip angle = 7°; $1 \times 1 \times 1\,mm^3$ voxels) and T2-weighted (TR/TE = 3200/412 ms, flip angle=120°; echo train length [ETL] = 258; $1 \times 1 \times 1\,mm^3$ voxels) Magnetic Resonance Imaging scan on a 3T Siemens Skyra scanner (Siemens AG, Erlangen, Germany) with a gradient of 45 mT/m and a maximum slew rate of 200 mT/m/s. The anatomical volume consisted of 160 sagittal slices of an isotropic voxel size ($1 \times 1 \times 1$ mm), covering the entire brain. The T1-weighted/T2-weighted corrected anatomical MRI was used to extract the scalp and cortical surfaces using a pipeline from the Human Connectome Project, detailed elsewhere[95]. This process yielded a surface triangulation for each envelope[96], resulting in individual high-resolution cortical surfaces with ~300,000 vertices per surface. These surfaces were then down-sampled to ~5000 vertices. In addition, a five-layer segmentation based on T1-weighted/T2-weighted corrected and T2-weighted images were performed using the algorithm implemented by the SimNIBS tool and SMP12.

Functional MRI data

During the fMRI experiment, functional images were acquired using a weighted echo-planar T2* sequence (TR/TE = 2390/35 ms, flip angle = 90°, $3 \times 3 \times 3$ mm voxels) while participants performed the MSIT task. The acquired volumes of each participant were then coregistered to the 2-mm standard imaging using the nonlinear algorithm, FNIRT, implemented in FMRIB Software Library (FSL)[97]. To analyze the imaging data, a model was used that isolated the activity associated with the expectancy of conflict using three regressors of interest: conflict stimuli, non-conflict stimuli, and conflict expectancy (Fig. 2). Second-level activation maps were calculated using a mixed-effects model in FSL, which evaluated two contrasts: conflict higher than no conflict and expectancy of conflict stimuli (Ex = Q, Fig. 2). Cluster correction was applied with a cluster threshold detection of $z > 3.1$ and a significance level of $p < 0.05$ using FLAME1.

TMS-EEG

The stimulation coordinates were individually set to each subject's brain space in both TMS-EEG sessions. One session was conducted according to the group peak in the SFG for Expectancy regressors, while the other was based on the IFJ for Conflict regressors (Fig. 2). A neuronavigation system was used to identify individual stimulation points (individual structural MRI scans, native space) in the nearest gray matter areas to the no-linear inverse co-registration of the individual anatomy (FSL algorithm, FNIRST) and restricted to be in A6/44d_L (SFG) and IFJ_L (IFJ) of Braintomme atlas segmentation[98]. TMS coil positioning and orientation regarding the brain x, y, and z axes (that is, yaw, pitch, and roll, respectively) were optimized so that the electric field impacted perpendicular to the target region, maximizing the induced current strength[72,99]. The stimulation intensity was set to the maximum tolerance level for each subject in this area, ranging from 80% to 120% of their motor threshold previously measured. This corresponds to a range of 30% to 60% of the machine's maximum intensity (mean = 40,6%, median = 39%). A 70-mm double coil (PMD70) was used for TMS pulses, which were delivered in three conditions: the theta condition (10 rhythmic pulses every 200 ms), the no-theta condition (10 arrhythmic pulses within 2 s), and the sham condition. Sham stimulation was performed in the same area but with the coil tilted, so participants did not receive actual stimulation. EEG recordings were obtained throughout the task in both sessions. We used TMS-compatible EEG equipment (BrainAmp 64 DC, BrainProducts, http://www.brainproducts.com/). EEG was continuously acquired from 64 channels (plus an acquisition reference (FCz) and a ground). TMS-compatible sintered Ag/AgCl-pin electrodes were used. The signal was band-pass filtered at DC to 1000 Hz and digitized at a sampling rate of 5000 Hz. Skin/electrode impedance was maintained below 5 kΩ. Electrode impedances were re-tested during pauses to ensure stable values throughout the experiment. The positions of the EEG electrodes were estimated using the neuronavigation system used for the TMS.

TMS electrophysiological analysis

For both stimulation sites, EEG power was modeled in two-time windows: one between the last TMS pulse and the first Go stimulus, and the other around Go stimuli. These analyses were performed using Matlab software's LAN package (https://github.com/neurocics/LAN_current) (https://matlab.mathworks.com/).

In the analysis between the last TMS pulse and the first Go stimuli, preprocessing was performed in multiple steps. We first detected the slow decay component of the TMS artifact. To this end, we segmented 3-s windows containing TMS pulses, automatically detected a period starting 10 ms pre to 20 ms post to the respective TMS peak, and removed this from the signal. We applied an Independent Component Analysis (ICA) to this signal using the Runica algorithm provided by the EEGLAB toolbox (https://sccn.ucsd.edu/eeglab/). Thus, we looked for a stereotype component with local bipolar distribution over the TMS site pulse and other psychological signals, such as blinking. In the second step, we segmented the raw signal in the time widows of analysis. We removed the segment between −10 and 30 ms around each TMS stimulation. We replaced it with an inverse-distance weighted interpolation [$Y = \text{sum}(X/D^3)/\text{sum}(1/D^3)$] plus a Gaussian noise with the standard deviation extracted to a reference period set to be 55 to −15 ms before the respective first TMS pulse and 0 of the mean. This procedure effectively removed the direct (non-physiological) and other TMS artifacts (e.g., TMS-locked artifacts at electrodes directly in contact with the TMS coil) without introducing discontinuities, essential for the later time-frequency analysis[69,72]. Following these steps, we down-sampled EEG data to 1000 Hz and used a

preprocessing pipeline developed for prior work[33,34,37,100–103]. The EEG data was then filtered 0.1–45 Hz band-pass and segmented −0.5 to 1.5 s around the last TMS pulse. The ICA calculated in the first step removed components such as TMS-related artifacts, blinks, and eye movement. Automatic artifact detection was used to remove noisy trials, including voltage threshold (150 µV and three std. dev.) and FFT-amplitude threshold (power spectrum greater than two std. dev. for more than 10% of the 0.5-to-40-Hz spectrum). A final manual review of all trials was performed to check for remaining noise trials, and mastoid electrodes were removed. A Morlet-type frequency analysis (5-cycle width) was performed, and a model with two dummy regressors, Theta TMS and No-Theta TMS, was fitted for each participant.

In the analysis around Go stimuli, data from each participant were preprocessed by decreasing the sampling rate to 1000. Go stimuli were segmented, noisy trials were removed by automatic artifact detection, and ICA was performed to remove blinks and eye movement. Mastoid electrodes were removed, and a manual review of all trials was carried out. The noisy channels were interpolated, and Morlet-type frequency analysis was performed.

For both time-windows of analysis, we conducted a first-level analysis using a general linear model over the power of each time-frequency bin in each EEG-TMS session separately, as described in our prior work. The power spectrum was normalized (dB) by a rest period recording at the beginning of each session. For the time-window between the last TMS pulse and the first Go stimulus, we used TMS_{theta} and $TMS_{no\text{-}theta}$ as regressors. For the time-window around the Go stimulus, we used a general linear model with seven regressors: Go, preceding Nogo error, preceding Go error, Expectancy, Expectancy*TMS interaction, Expectancy*TMS_{theta} interaction, TMS, TMS_{theta}. Then, for each session, the normalized beta value of each regressor (beta values/standard error) in each time-frequency bin was used in the second-level analysis. In this analysis, consistent modulation (or consistent differences between TMS sessions, i.e., between IFJ and SFG sessions) across subjects were tested in each bin using the Wilcoxon test. Then, the uncorrected significant differences were corrected for multiple comparisons using a cluster-based permutation test.

Cluster-based permutation test

We employed a cluster-based permutation test to address multiple comparisons in our time-frequency analysis[104]. Significant regions were identified by clustering neighboring sites showing the same effect (with a significance level of $p < 0.05$ in the statistical tests applied to either the time-frequency chart or the sources, such as the Wilcoxon test). Cluster-level statistics were computed as the sum of statistics from all sites within the cluster. We evaluated the significance of these clusters by comparing them to the largest cluster-level statistics in a permutation distribution. This distribution was generated by randomly permuting the original data. Specifically, we created null models for each participant, maintaining the original model structure while permuting the tested regressor. Following each permutation, we conducted the initial statistical test (e.g., Wilcoxon) and recorded the cluster-level statistics of the largest cluster from the permutation distribution. After 5000 permutations, we estimated the cluster-level significance for each observed cluster as the proportion of values in the permutation distribution surpassing the cluster-level statistics of the corresponding cluster. For all time-frequency results, we highlighted all clusters that presented a p-corrected <0.05. We indicated the highest p-value highlighted in each time-frequency chart to present more precise information.

EEG source estimation

We estimated the neural current density time series at each brain location using a minimum norm estimate inverse solution LORETA algorithm with unconstrained dipole orientations. This estimation was performed individually for each trial, condition, and subject, employing Brainstorm software[105]. We used a tessellated cortical mesh to model the brain based on each individual's anatomy. This mesh was employed to estimate the distribution of current sources, with ~3 × 8000 sources positioned on the segmented cortical surface (three orthogonal sources at each spatial location). We employed a five-layer continuous Galerkin finite element conductivity model, as implemented in DUneuro software[106], along with a physical forward model. We multiplied the recorded raw EEG time series from the electrodes by the inverse operator to obtain cortical activity estimates at the cortical sources. This operation yielded the estimated source current at the cortical surface as a function of time. Importantly, this transformation is linear and does not alter the frequencies of the underlying sources, enabling us to conduct time-frequency analyses directly in the source space. Within this source space, we simplified each vertex's dipole to one by selecting the component with the highest variance, employing the PCA algorithm. Subsequently, we performed frequency decomposition using the Wavelets transform. To ensure the reliability of our results, we only present source estimations if statistically significant differences are observed at both the electrode and source levels, thereby accounting for multiple comparison corrections.

Software

For stimulus presentation, we used Presentation (v18, Neurobehavioral Systems). BrainVision Recorder was used to coordinate stimulus presentation, EEG and TMS pulse delivery. fMRI analyses were conducted using FSL 6.0.6. EEG analyses were performed with LAN toolbox (v1.9.9), Brainstorm 3, DUneuro software (http://duneuro.org/), and the SimNIBS tool (RRID: SCR_014109). Statistical analyses were implemented in R 4.2.1 and JAGS 4.3.0

Reporting summary

Further information on research design is available in the Nature Portfolio Reporting Summary linked to this article.

Data availability

The behavioral data generated in this study are provided in the Supplementary Information/Source Data file and are available in a public repository on zenodo (https://doi.org/10.5281/zenodo.13919426). The neuronal data generated in this study are available in a public repository on openNEURO (https://doi.org/10.18112/openneuro.ds005571.v1.0.0) Source data are provided with this paper.

Code availability

All codes are available on Zenodo under the following https://doi.org/10.5281/zenodo.13919426 and https://doi.org/10.5281/zenodo.13923690.

References

1. Braver, T. S. The variable nature of cognitive control: a dual mechanisms framework. *Trends Cogn. Sci.* **16**, 106–113 (2012).
2. Koechlin, E., Ody, C. & Kouneiher, F. The architecture of cognitive control in the human prefrontal. *Cortex Sci.* **302**, 1181–1185 (2003).
3. Collins, A. G. E. & Shenhav, A. Advances in modeling learning and decision-making in neuroscience. *Neuropsychopharmacology* 1–15 https://doi.org/10.1038/s41386-021-01126-y (2021).
4. Koechlin, E. An evolutionary computational theory of prefrontal executive function in decision-making. *Philos. Trans. R. Soc. B Biol. Sci.* **369**, 20130474 (2014).
5. Aron, A. R. From reactive to proactive and selective control: developing a richer model for stopping inappropriate responses. *Biol. Psychiat.* **69**, e55–e68 (2010).
6. Hannah, R. & Aron, A. R. Towards real-world generalizability of a circuit for action-stopping. *Nat. Rev. Neurosci.* **22**, 538–552 (2021).

7. Zamorano, F. et al. Lateral prefrontal theta oscillations reflect proactive cognitive control impairment in males with attention deficit hyperactivity disorder. *Front. Syst. Neurosci.* **14**, 37 (2020).
8. Vanderhasselt, M.-A. et al. Abnormal proactive and reactive cognitive control during conflict processing in major depression. *J. Abnorm. Psychol.* **123**, 68–80 (2014).
9. Sun, N. et al. Fractional amplitude of low-frequency fluctuations and gray matter volume alterations in patients with bipolar depression. *Neurosci. Lett.* **730**, 135030 (2020).
10. Fruehauf, L. M., Fair, J. E., Liebel, S. W., Bjornn, D. & Larson, M. J. Cognitive control in obsessive-compulsive disorder (OCD): Proactive control adjustments or consistent performance? *Psychiatry Res.* **298**, 113809 (2021).
11. Kricheldorff, J., Ficke, J., Debener, S. & Witt, K. Impaired proactive cognitive control in Parkinson's disease. *Brain Commun.* **5**, fcad327 (2023).
12. Fan, Y. et al. Grey matter volume and its association with cognitive impairment and peripheral cytokines in excited individuals with schizophrenia. *Brain Imaging Behav.* **16**, 2618–2626 (2022).
13. Qiu, X. et al. The relationship between abnormal resting-state functional connectivity of the left superior frontal gyrus and cognitive impairments in youth-onset drug-naïve schizophrenia. *Front. Psychiatry* **12**, 679642 (2021).
14. Lesh, T. A. et al. Proactive and reactive cognitive control and dorsolateral prefrontal cortex dysfunction in first episode schizophrenia. *NeuroImage Clin.* **2**, 590–599 (2013).
15. Töllner, T. et al. Two Independent frontal midline theta oscillations during conflict detection and adaptation in a simon-type manual reaching task. *J. Neurosci.* **37**, 2504–2515 (2017).
16. Schmidt, J. R. Questioning conflict adaptation: proportion congruent and Gratton effects reconsidered. *Psychon. Bull. Rev.* **20**, 615–630 (2013).
17. Horga, G. et al. Adaptation to conflict via context-driven anticipatory signals in the dorsomedial prefrontal cortex. *J. Neurosci.* **31**, 16208–16216 (2011).
18. Grundy, J. G. The specificity and reliability of conflict adaptation: a mouse-tracking study. *Front. Psychol.* **12**, 770509 (2022).
19. Bugg, J. M. Opposing influences on conflict-driven adaptation in the Eriksen flanker task. *Mem. Cogn.* **36**, 1217–1227 (2008).
20. Schmidt, J. R. Evidence against conflict monitoring and adaptation: an updated review. *Psychon. Bull. Rev.* **26**, 753–771 (2019).
21. Braem, S., Abrahamse, E. L., Duthoo, W. & Notebaert, W. What determines the specificity of conflict adaptation? A review, critical analysis, and proposed synthesis. *Front. Psychol.* **5**, 1134 (2014).
22. Karayanidis, F., Whitson, L. R., Heathcote, A. & Michie, P. T. Variability in proactive and reactive cognitive control processes across the adult lifespan. *Front. Psychol.* **2**, 318 (2011).
23. Alzahabi, R., Hussey, E. & Ward, N. The influence of context representations on cognitive control states. *Cogn. Res. Princ. Implic.* **7**, 93 (2022).
24. Yang, Q. & Pourtois, G. Reduced flexibility of cognitive control: reactive, but not proactive control, underpins the congruency sequence effect. *Psychol. Res.* **86**, 474–484 (2022).
25. Liebrand, M., Pein, I., Tzvi, E. & Krämer, U. M. Temporal dynamics of proactive and reactive motor inhibition. *Front. Hum. Neurosci.* **11**, 204 (2017).
26. Egner, T. Principles of cognitive control over task focus and task switching. *Nat. Rev. Psychol.* **2**, 702–714 (2023).
27. Braem, S. et al. Measuring adaptive control in conflict tasks. *Trends Cogn. Sci.* **23**, 769–783 (2019).
28. Jiang, J., Heller, K. & Egner, T. Bayesian modeling of flexible cognitive control. *Neurosci. Biobehav. Rev.* **46**, 30–43 (2014).
29. Donoso, M., Collins, A. G. E. & Koechlin, E. Foundations of human reasoning in the prefrontal cortex. *Science* **344**, 1481–1486 (2014).
30. Koechlin, E., Basso, G., Pietrini, P., Panzer, S. & Grafman, J. The role of the anterior prefrontal cortex in human cognition. *Nature* **399**, 148–151 (1999).
31. Magis-Weinberg, L., Custers, R. & Dumontheil, I. Rewards enhance proactive and reactive control in adolescence and adulthood. *Soc. Cogn. Affect. Neurosci.* **14**, 1219–1232 (2019).
32. Cavanagh, J. F. & Frank, M. J. Frontal theta as a mechanism for cognitive control. *Trends Cogn. Sci.* **18**, 414–421 (2014).
33. Lavín, C., Soto-Icaza, P., López, V. & Billeke, P. Another in need enhances prosociality and modulates frontal theta oscillations in young adults. *Front. Psychiatry* **14**, 1160209 (2023).
34. Figueroa-Vargas, A. et al. Frontoparietal connectivity correlates with working memory performance in multiple sclerosis. *Sci. Rep.* **10**, 9310 (2020).
35. Billeke, P., Zamorano, F., Cosmelli, D. & Aboitiz, F. Oscillatory brain activity correlates with risk perception and predicts social decisions. *Cereb. Cortex* **23**, 2872–2883 (2013).
36. Billeke, P. et al. Someone has to give in: theta oscillations correlate with adaptive behavior in social bargaining. *Soc. Cogn. Affect Neurosci.* **9**, 2041–2048 (2014).
37. Larrain-Valenzuela, J. et al. Theta and alpha oscillation impairments in autistic spectrum disorder reflect working memory deficit. *Sci. Rep.* **7**, 14328 (2017).
38. Driel, J., van, Swart, J. C., Egner, T., Ridderinkhof, K. R. & Cohen, M. X. (No) time for control: Frontal theta dynamics reveal the cost of temporally guided conflict anticipation. *Cogn. Affect. Behav. Neurosci.* **15**, 787–807 (2015).
39. Chang, A., Ide, J. S., Li, H.-H., Chen, C.-C. & Li, C.-S. R. Proactive control: neural oscillatory correlates of conflict anticipation and response slowing. *Eneuro* **4**, ENEURO.0061–17.2017 (2017).
40. Zamorano, F. et al. Temporal constraints of behavioral inhibition: relevance of inter-stimulus interval in a go-nogo task. *PLoS ONE* **9**, e87232 (2014).
41. Gratton, G., Coles, M. G. H. & Donchin, E. Optimizing the use of information: strategic control of activation of responses. *J. Exp. Psychol. Gen.* **121**, 480–506 (1992).
42. Gratton, G., Cooper, P., Fabiani, M., Carter, C. S. & Karayanidis, F. Dynamics of cognitive control: theoretical bases, paradigms, and a view for the future. *Psychophysiology* **55**, 1–25 (2018).
43. Vandekerckhove, J., Tuerlinckx, F. & Lee, M. D. Hierarchical diffusion models for two-choice response times. *Psychol. Methods* **16**, 44–62 (2011).
44. Desender, K., Boldt, A., Verguts, T. & Donner, T. H. Confidence predicts speed-accuracy tradeoff for subsequent decisions. *eLife* **8**, e43499 (2019).
45. Fu, Z. et al. The geometry of domain-general performance monitoring in the human medial frontal cortex. *Science* **376**, 1–10 (2022).
46. Buonomano, D. V., Bramen, J. & Khodadadifar, M. Influence of the interstimulus interval on temporal processing and learning: testing the state-dependent network model. *Philos. Trans. R. Soc. B Biol. Sci.* **364**, 1865–1873 (2009).
47. Francis, G. Cortical dynamics of lateral inhibition: Visual persistence and ISI. *Percept. Psychophys.* **58**, 1103–1109 (1996).
48. Zamorano, F. et al. Lateral prefrontal activity as a compensatory strategy for deficits of cortical processing in attention deficit hyperactivity disorder. *Sci. Rep.* **7**, 7181 (2017).
49. Barber, A. D., Caffo, B. S., Pekar, J. J. & Mostofsky, S. H. Effects of working memory demand on neural mechanisms of motor response selection and control. *J. Cogn. Neurosci.* **25**, 1235–1248 (2013).
50. Sundermann, B. & Pfleiderer, B. Functional connectivity profile of the human inferior frontal junction: involvement in a cognitive control network. *BMC Neurosci.* **13**, 119–119 (2012).

51. Helfrich, R. F. & Knight, R. T. Oscillatory dynamics of prefrontal cognitive control. *Trends Cogn. Sci.* **20**, 916–930 (2016).
52. Wyart, V., de Gardelle, V., Scholl, J. & Summerfield, C. Rhythmic fluctuations in evidence accumulation during decision making in the human brain. *Neuron* **76**, 847–858 (2012).
53. Arnal, L. H., Doelling, K. B. & Poeppel, D. Delta–beta coupled oscillations underlie temporal prediction accuracy. *Cereb. Cortex* **25**, 3077–3085 (2015).
54. Riddle, J., McFerren, A. & Frohlich, F. Causal role of cross-frequency coupling in distinct components of cognitive control. *Prog. Neurobiol.* **202**, 102033 (2021).
55. Hu, S., Ide, J. S., Zhang, S. & Li, C. R. Anticipating conflict: neural correlates of a Bayesian belief and its motor consequence. *NeuroImage* **119**, 286–295 (2015).
56. Hu, J. et al. Novelty seeking, harm avoidance, and cerebral responses to conflict anticipation: an exploratory study. *Front. Hum. Neurosci.* **10**, 546 (2016).
57. Jiang, J., Beck, J., Heller, K. & Egner, T. An insula-frontostriatal network mediates flexible cognitive control by adaptively predicting changing control demands. *Nat. Commun.* **6**, 8165 (2015).
58. McLoughlin, G., Gyurkovics, M., Palmer, J. & Makeig, S. Midfrontal theta activity in psychiatric illness: an index of cognitive vulnerabilities across disorders. *Biol. Psychiatry* **91**, 173–182 (2022).
59. Koechlin, E. & Summerfield, C. An information theoretical approach to prefrontal executive function. *Trends Cogn. Sci.* **11**, 229–235 (2007).
60. Yang, G. et al. Distinct brain mechanisms for conflict adaptation within and across conflict types. *J. Cogn. Neurosci.* **34**, 445–460 (2022).
61. Rahnev, D., Nee, D. E., Riddle, J., Larson, A. S. & D'Esposito, M. Causal evidence for frontal cortex organization for perceptual decision making. *Proc. Natl Acad. Sci.* **113**, 6059–6064 (2016).
62. García, M.B., Grueschow, M., Moisa, M., Polania, R. & Ruff, C.C. Causal evidence for a domain-specific role of left superior frontal sulcus in human perceptual decision Preprint at *eLife* **13**, https://doi.org/10.7554/eLife.94576.1 (2024).
63. Yu, S., Mückschel, M. & Beste, C. Superior frontal regions reflect the dynamics of task engagement and theta band-related control processes in time-on task effects. *Sci. Rep.* **12**, 846 (2022).
64. Schroeter, M. L., Eickhoff, S. B. & Engel, A. From correlational approaches to meta-analytical symptom reading in individual patients: Bilateral lesions in the inferior frontal junction specifically cause dysexecutive syndrome. *Cortex* **128**, 73–87 (2020).
65. Muhle-Karbe, P. S. et al. Co-activation-based parcellation of the lateral prefrontal cortex delineates the inferior frontal junction area. *Cereb. Cortex* **26**, 2225–2241 (2016).
66. Tagliaferri, M., Giampiccolo, D., Parmigiani, S., Avesani, P. & Cattaneo, L. Connectivity by the frontal aslant tract (FAT) explains local functional specialization of the superior and inferior frontal gyri in humans when choosing predictive over reactive strategies: a tractography-guided TMS study. *J. Neurosci.* **43**, 6920–6929 (2023).
67. Pulopulos, M. M. et al. Neuromodulation special issue effects of HF-rTMS over the left and right DLPFC on proactive and reactive cognitive control. *Soc. Cogn. Affect. Neurosci.* **17**, 109–119 (2020).
68. Plas, M., van der, Braun, V., Stauch, B. J. & Hanslmayr, S. Stimulation of the left dorsolateral prefrontal cortex with slow rTMS enhances verbal memory formation. *PLoS Biol.* **19**, e3001363 (2021).
69. Albouy, P., Weiss, A., Baillet, S. & Zatorre, R. J. Selective entrainment of theta oscillations in the dorsal stream causally enhances auditory working memory performance. *Neuron* **94**, 193–206.e5 (2017).
70. Bagherzadeh, Y., Khorrami, A., Zarrindast, M. R., Shariat, S. V. & Pantazis, D. Repetitive transcranial magnetic stimulation of the dorsolateral prefrontal cortex enhances working memory. *Exp. Brain Res.* **234**, 1807–1818 (2016).
71. Martin, D. M. et al. Individualised Transcranial magnetic stimulation targeting of the left dorsolateral prefrontal cortex for enhancing cognition: a randomised controlled trial. *Brain Sci.* **14**, 299 (2024).
72. Thut, G. et al. Rhythmic TMS causes local entrainment of natural oscillatory signatures. *Curr. Biol.* **21**, 1176–1185 (2011).
73. Senoussi, M. et al. Theta oscillations shift towards optimal frequency for cognitive control. *Nat. Hum. Behav.* **6**, 1000–1013 (2022).
74. Groppa, S. et al. Subcortical substrates of TMS induced modulation of the cortico-cortical connectivity. *Brain Stimul.* **6**, 138–146 (2013).
75. Eldaief, M. C. et al. Network-specific metabolic and haemodynamic effects elicited by non-invasive brain stimulation. *Nat. Ment. Heal.* **1**, 346–360 (2023).
76. Momi, D. et al. Perturbation of resting-state network nodes preferentially propagates to structurally rather than functionally connected regions. *Sci. Rep.* **11**, 12458 (2021).
77. Jargow, J., Zwosta, K., Korb, F. M., Ruge, H. & Wolfensteller, U. Low-frequency TMS results in condition-related dynamic activation changes of stimulated and contralateral inferior parietal lobule. *Front. Hum. Neurosci.* **15**, 684367 (2021).
78. Andoh, J. & Zatorre, R. J. Mapping interhemispheric connectivity using functional MRI after transcranial magnetic stimulation on the human auditory cortex. *NeuroImage* **79**, 162–171 (2013).
79. Zazio, A., Miniussi, C. & Bortoletto, M. Alpha-band cortico-cortical phase synchronization is associated with effective connectivity in the motor network. *Clin. Neurophysiol.* **132**, 2473–2480 (2021).
80. Hare, S. M. et al. Mapping local and long-distance resting connectivity markers of TMS-related inhibition reduction in schizophrenia. *NeuroImage Clin.* **31**, 102688 (2021).
81. Sydnor, V. J. et al. Cortical-subcortical structural connections support transcranial magnetic stimulation engagement of the amygdala. *Sci. Adv.* **8**, eabn5803 (2022).
82. Gießing, C., Alavash, M., Herrmann, C. S., Hilgetag, C. C. & Thiel, C. M. Individual differences in local functional brain connectivity affect TMS effects on behavior. *Sci. Rep.* **10**, 10422 (2020).
83. Rafiei, F. & Rahnev, D. TMS does not increase BOLD activity at the site of stimulation: a review of all concurrent TMS-fMRI studies. *eNeuro* **9**, ENEURO.0163–22.2022 (2022).
84. Oehrn, C. R. et al. Neural communication patterns underlying conflict detection, resolution, and adaptation. *J. Neurosci.* **34**, 10438–10452 (2014).
85. Chen, K.-H. et al. Theta low-gamma phase amplitude coupling in the human orbitofrontal cortex increases during a conflict-processing task. *J. Neural Eng.* **19**, 016026 (2022).
86. Harrewijn, A. et al. Electrocortical measures of information processing biases in social anxiety disorder: a review. *Biol. Psychol.* **129**, 324–348 (2017).
87. Kazemi, R. et al. Alpha frequency rTMS modulates theta lagged nonlinear connectivity in dorsal attention network. *Brain Res. Bull.* **162**, 271–281 (2020).
88. Riddle, J., Scimeca, J. M., Cellier, D., Dhanani, S. & D'Esposito, M. Causal evidence for a role of theta and alpha oscillations in the control of working memory. *Curr. Biol.* **30**, 1748–1754.e4 (2020).
89. Figueroa-Vargas, A. et al. The effect of a cognitive training therapy based on stimulation of brain oscillations in patients with mild cognitive impairment in a Chilean sample: study protocol for a phase IIb, 2 × 3 mixed factorial, double-blind randomised controlled trial. *Trails* **25**, 1–14 (2024).
90. Soto-Icaza, P. et al. Oscillatory activity underlying cognitive performance in children and adolescents with autism: a systematic review. *Front. Hum. Neurosci.* **18**, 1320761 (2024).

91. Soto-Icaza, P., Beffara-Bret, B., Vargas, L., Aboitiz, F. & Billeke, P. Differences in cortical processing of facial emotions in broader autism phenotype. *PLoS ONE* **17**, e0262004 (2022).
92. Ratcliff, R., Huang-Pollock, C. & McKoon, G. Modeling individual differences in the Go/No-Go task with a diffusion model. *Decision* **5**, 42–62 (2018).
93. Lerche, V. & Voss, A. Experimental validation of the diffusion model based on a slow response time paradigm. *Psychol. Res.* **83**, 1194–1209 (2019).
94. Kausel, L. et al. Patients recovering from COVID-19 who presented with anosmia during their acute episode have behavioral, functional, and structural brain alterations. *Sci. Rep.* **14**, 19049 (2024).
95. Glasser, M. F. et al. The minimal preprocessing pipelines for the Human Connectome Project. *NeuroImage* **80**, 105–124 (2013).
96. Fischl, B. FreeSurfer. *Neuroimage* **62**, 774–781 (2012).
97. Jenkinson, M., Beckmann, C. F., Behrens, T. E. J., Woolrich, M. W. & Smith, S. M. FSL. *NeuroImage* **62**, 782–790 (2012).
98. Fan, L. et al. The human brainnetome atlas: a new brain atlas based on connectional architecture. *Cereb. Cortex* **26**, 3508–3526 (2016).
99. Valero-Cabré, A., Amengual, J. L., Stengel, C., Pascual-Leone, A. & Coubard, O. A. Transcranial magnetic stimulation in basic and clinical neuroscience: a comprehensive review of fundamental principles and novel insights. *Neurosci. Biobehav Rev.* **83**, 381–404 (2017).
100. Soto-Icaza, P., Vargas, L., Aboitiz, F. & Billeke, P. Beta oscillations precede joint attention and correlate with mentalization in typical development and autism. *Cortex* **113**, 210–228 (2019).
101. Billeke, P. et al. Paradoxical expectation: oscillatory brain activity reveals social interaction impairment in schizophrenia. *Biol. Psychiatry* **78**, 421–431 (2014).
102. Billeke, P., Zamorano, F., Chavez, M., Cosmelli, D. & Aboitiz, F. Functional cortical network in alpha band correlates with social bargaining. *PLoS ONE* **9**, e109829 (2014).
103. Valdebenito-Oyarzo, G. et al. The parietal cortex has a causal role in ambiguity computations in humans. *PLoS Biol.* **22**, e3002452 (2024).
104. Maris, E. & Oostenveld, R. Nonparametric statistical testing of EEG- and MEG-data. *J. Neurosci. Methods* **164**, 177–190 (2007).
105. Tadel, F., Baillet, S., Mosher, J. C., Pantazis, D. & Leahy, R. M. Brainstorm: a user-friendly application for MEG/EEG analysis. *Comput. Intel. Neurosci.* **2011**, 879716 (2010).
106. Medani, T. et al. Brainstorm-DUNEuro: an integrated and user-friendly Finite Element Method for modeling electromagnetic brain activity. *NeuroImage* **267**, 119851 (2023).

Acknowledgements

We thank all the participants who generously participated in this research. We thank all the research staff involved in participant recruitment, data collection, and database administration. Funding Support: Agencia Nacional de Investigación y Desarrollo de Chile (ANID), FONDECYT (1181295 and 1211227 to P.B.), PAI (PAI77190047 to P.S-I), FONDEQUIP (EQM150076 to P.B.).

Author contributions

Conceptualization, P.B., M.M-M., A.V-C. and R.P.; Methodology, P.B., R.P., and M.M-M.; Formal Analysis, P.B., M.M-M. and R.P., Investigation M.M-M., G.V-O., A.F-V., P.C-P, and P.B.; Resources F.Z., C.S., and X.S.; Writing P.B., P.S-I., M.M-M., and R.P. Project Administration P.B., M.M-M. and A.F-V.; Funding Acquisition P.B., and P.S-I.

Competing interests

The authors declare no competing interests.

Additional information

Supplementary information The online version contains supplementary material available at https://doi.org/10.1038/s41467-024-54244-8.

Correspondence and requests for materials should be addressed to Pablo Billeke.

Peer review information *Nature Communications* thanks James Cavanagh and the other, anonymous, reviewer(s) for their contribution to the peer review of this work. A peer review file is available.